

SOLUTION-BASED SYNTHESIS OF SILVER-PLATINUM CORE-SHELL
NANOWIRES WITH ENHANCED STABILITY

A THESIS SUBMITTED TO
THE GRADUATE SCHOOL OF NATURAL AND APPLIED SCIENCES
OF
MIDDLE EAST TECHNICAL UNIVERSITY

BY

SERKAN KOYLAN

IN PARTIAL FULFILLMENT OF THE REQUIREMENTS
FOR
THE DEGREE OF MASTER OF SCIENCE
IN
METALLURGICAL AND MATERIALS ENGINEERING

SEPTEMBER 2019

Approval of the thesis:

**SOLUTION-BASED SYNTHESIS OF SILVER-PLATINUM CORE-SHELL
NANOWIRES WITH ENHANCED STABILITY**

submitted by **SERKAN KOYLAN** in partial fulfillment of the requirements for the degree of **Master of Science in Metallurgical and Materials Engineering Department, Middle East Technical University** by,

Prof. Dr. Halil Kalıpçılar
Dean, Graduate School of **Natural and Applied Sciences**

Prof. Dr. Cemil Hakan Gür
Head of Department, **Met. and Mat. Eng.**

Prof. Dr. Hüsnü Emrah Ünalın
Supervisor, **Met. and Mat. Eng., METU**

Assist. Prof. Dr. Simge Çınar
Co-Supervisor, **Met. And Mat. Eng, METU**

Examining Committee Members:

Assoc. Prof. Dr. Emrullah Görkem Günbař
Department of Chemistry, METU

Prof. Dr. Hüsnü Emrah Ünalın
Met. and Mat. Eng., METU

Assist. Prof. Dr. Simge Çınar
Met. and Mat. Eng., METU

Assist. Prof. Dr. řahin Cořkun
Met. and Mat. Eng., Eskiřehir Osmangazi Uni.

Assist. Prof. Dr. Selçuk Yerci
Micro and Nanotechnology, METU

Date: 06.09.2019

I hereby declare that all information in this document has been obtained and presented in accordance with academic rules and ethical conduct. I also declare that, as required by these rules and conduct, I have fully cited and referenced all material and results that are not original to this work.

Name, Surname: Serkan Koylan

Signature:

ABSTRACT

SOLUTION-BASED SYNTHESIS OF SILVER-PLATINUM CORE-SHELL NANOWIRES WITH ENHANCED STABILITY

Koylan, Serkan

Master of Science, Metallurgical and Materials Engineering

Supervisor: Prof. Dr. Hüsnü Emrah Ünalın

Co-Supervisor: Assist. Prof. Dr. Simgė Çınar

September 2019, 76 pages

This work describes a facile route for the synthesis of silver (Ag)-platinum (Pt) core-shell nanowires (NWs) with controlled diameter in the range of 63-96 nm. Optimum synthesis conditions were determined to obtain conformal and galvanic replacement free deposition of Pt on Ag NWs. Synthesized Ag-Pt core-shell NWs were examined using SEM, TEM and XPS.

Further studies were conducted to compare the performances of Ag-Pt core-shell NW networks to those of pristine Ag NW networks. In this regard, electrochemical, chemical and environmental stabilities were elaborated. Electrochemical stability tests were conducted in three electrode configuration comprised of Ag/AgCl reference, Pt plate counter and nanowire network working electrodes. In chemical stability tests, resistance change upon hydrogen peroxide exposure was monitored. The environmental stability tests were carried out under different relative humidity levels and temperatures. The humidity levels and temperatures were selected as 43, 75 and 84 %RH and 150 °C, 75 °C and room temperature, respectively.

In all cases, clear improvement of stability for Ag-Pt core-shell NW networks were obtained. All in all, this highly effective and simple strategy to improve the stability

of Ag NWs will certainly open new avenues for their large scale utilization in various optoelectronic devices.

Keywords: Silver-Platinum Core-Shell Nanowires, Environmental Stability, Electrochemical Stability

ÖZ

KARARLILIĞI ARTTIRILMIŞ GÜMÜŞ-PLATİN ÇEKİRDEK-KABUK NANOTELLERİN ÇÖZELTİ BAZLI SENTEZİ

Koylan, Serkan
Yüksek Lisans, Metalurji ve Malzeme Mühendisliği
Tez Danışmanı: Prof. Dr. Hüsnü Emrah Ünalın
Ortak Tez Danışmanı: Dr. Öğr. Üyesi Simge Çınar

Eylül 2019, 76 sayfa

Bu çalışmada, 63-92 nm çapa sahip gümüş (Ag)-platin (Pt) çekirdek-kabuk nanotellerin kontrollü sentezi için uygun bir yol sunulmaktadır. Ag nanotellerin, konformal ve galvanik yer değiştirme olmadan Pt ile kaplanması için optimum koşullar belirlenmiştir. Sentezlenen Ag-Pt çekirdek-kabuk nanoteller SEM, TEM ve XPS yöntemleri ile incelenmiştir.

Yapılan çalışmalar, Ag-Pt çekirdek-kabuk nanotel ağının performansını, Ag nanotel ağı ile karşılaştırmak için derine indirilmiştir. Bu bağlamda, elektrokimyasal, kimyasal ve çevresel kararlılıkları belirleyici yollar üzerinde durulmuştur. Elektrokimyasal kararlılık ölçümleri, Ag/AgCl'nin referans elektrot, Pt plakanın karşıt elektrot ve nanotel ağının oluşan çalışma elektrotu olarak kullanıldığı üç elektrot ölçüm biçimiyle yapılmıştır. Kimyasal kararlılık testlerinde, hidrojen peroksit maruz bırakılan elektrotların direnç değişimi ölçülmüştür. Çevresel kararlılık testleri, farklı bağıl nem seviyeleri ve sıcaklıklar üzerinde gerçekleştirilmiştir. Nem seviyeleri ve sıcaklıklar sırasıyla % 43, 75 ve % 84 bağıl nem ile 150 °C, 75 °C ve oda sıcaklığı seçilmiştir.

Yapılan tüm karşılaştırmalarda, kararlılıkta iyileşme Ag-Pt çekirdek-kabuk nanotel ağı ile açıkça elde edilmiştir. Yapılan çalışmalar göz önüne alındığında, Ag nanotel

ađının kararlılıđını arttırmak için geliştirilen bu çok etkili ve kolay yöntem, geniş çapta farklı optik-elektronik cihaz uygulamalarında yeni yolları kesinlikle açacaktır.

Anahtar Kelimeler: Gümüş-Platin Çekirdek-Kabuk Nanotl, Çevresel Kararlılık, Elektrokimyasal Kararlılık

To those of people who are very valuable for me

ACKNOWLEDGEMENTS

This work was supported by the Scientific and Technological Research Council of Turkey (TUBITAK) under Grant No. 117E539.

Firstly, I would like to express my deepest appreciation to my advisor Prof. Dr. H. Emrah Ünal for his patience and guidance during my studies. I am also thankful to him for accepting his laboratory and involving the project.

I always feel very lucky to have a project partner. In the most difficult times, I always found Şensu Tunca with me trying to motivate me. She never gave up making me laugh.

I would like to express my gratitude to Doğa Doğanay and Mete Batuhan Durukan for encouraging to finish the thesis and completing some of my measurements.

I thank to Dr. Şahin Coşkun and Gökhan Polat for guidance in the academic life and teaching life lessons. They always wanted what was the best for me.

I would like to thank my lab mates Merve Nur Güven, Alptekin Aydın, Yusuf Tütel, Dr. Ferzaneh Hekmat, Efe Boyacıgiller, Elif Özlem Güner, Şeyma Koç, Can Çuhadar, Umur Balım, Ogeday Çiçek, Caner Görür and Alptuğ Calasın. I am also grateful to Sevim Polat, Doğanca Tigan, Dr. Recep Yüksel and Ece Alpuğan for sharing their experiences in Nanolab.

I would like to thank our project partners Prof. Seung Hwan Ko and his PhD. student Dongkwan Kim from Seoul National University for both TEM and SEM analyses and their collaboration.

Lastly, I would like to thank Özlem Ünal going into my life. She will always be in my good memories.

TABLE OF CONTENTS

ABSTRACT	v
ÖZ	vii
ACKNOWLEDGEMENTS.....	x
TABLE OF CONTENTS	xi
LIST OF TABLES.....	xv
LIST OF FIGURES	xvi
LIST OF ABBREVIATIONS.....	xxi
LIST OF SYMBOLS	xxiii
CHAPTERS	
1. INTRODUCTION.....	1
2. SILVER PLATINUM CORE SHELL NANOWIRES	3
2.1. Synthesis of Ag NWs.....	3
2.1.1. Polyol Method	3
2.1.1.1. Effect of Silver Nitrate Concentration	5
2.1.1.2. Effect of Polyvinylpyrrolidone (PVP) Concentration	7
2.1.1.3. Effect of Metal Salts	8
2.2. Coating of Nanowires	10
2.2.1. Metal Coating.....	11
2.2.2. Oxide Coating.....	13
2.2.3. Polymer Coating.....	14
2.2.4. Hybrid Structures with Carbon-Based Materials	15
2.3. Experimental Procedure.....	17

2.3.1. Synthesis of Ag NWs.....	18
2.3.2. Synthesis of Ag-Pt Core-Shell NWs.....	19
2.4. Nanowire Characterization Methods.....	20
2.4.1. Scanning Electron Microscope (SEM)	20
2.4.2. Transmission Electron Microscope (TEM)	21
2.4.3. X-Ray Diffraction Analysis (XRD).....	21
2.4.4. X-Ray Photoelectron Spectroscopy (XPS).....	21
2.4.5. pH Measurements	21
2.5. Results	22
2.5.1. Bare Silver Nanowires	22
2.5.2. Ag-Pt Core-Shell NWs	23
3. SILVER PLATINUM CORE SHELL NANOWIRE NETWORKS WITH ENHANCED STABILITY	39
3.1. Stability of NW Networks	39
3.1.1. Electrochemical Stability.....	39
3.1.2. Environmental Stability	42
3.1.3. Chemical Stability.....	42
3.1.4. Thermal Stability	43
3.1.5. Mechanical Stability	44
3.2. Experimental Procedure	45
3.2.1. Electrode Preparation.....	45
3.3. Characterization Methods.....	45
3.3.1. Scanning Electron Microscope (SEM)	45
3.3.2. Electrochemical Measurements	45

3.3.3. Relative Humidity	46
3.4. Results.....	46
3.4.1. Environmental Stability.....	46
3.4.1.1. Temperature Stability	46
3.4.1.2. Relative Humidity.....	48
3.4.1.3. Chemical Stability	50
3.4.2. Electrochemical Stability	51
4. SILVER-PLATINUM CORE-SHELL NANOWIRE NETWORKS BASED THIN FILM HEATERS	55
4.1. Introduction.....	55
4.2. Random Network Formation	55
Thin Film Heaters	56
4.3.....	56
4.3.1. Working Principles.....	56
4.3.2. Results from Literature.....	58
4.4. Experimental Procedure.....	60
4.4.1. Electrode Preparation	60
4.5. Characterization Methods	60
4.5.1. Scanning Electron Microscope (SEM).....	60
4.5.2. Thin Film Heater	61
4.6. Results.....	61
Performance of Thin Film Heaters	61
4.6.1.....	61
5. CONCLUSIONS AND FUTURE RECOMMENDATIONS	65

5.1. Conclusions	65
5.2. Future Recommendations	66
REFERENCES.....	67
APPENDICES	75

LIST OF TABLES

TABLES

Table 2. 1 Investigated parameters and the reasoning.....	20
Table 2. 2 Average diameter and relative atomic percentage for Ag and Pt obtained from synthesis using different chloroplatinic acid amount.....	31
Table 4. 1 Measured temperature values for different applied voltages and corresponding current values.....	63

LIST OF FIGURES

FIGURES

- Figure 2. 1 (a) SEM image of Ag NWs synthesized by polyol method for the first time [5] (b) Schematic drawings of growth mechanism of Ag NWs; penta-twinned Ag NWs formation from nanorod (top) and reduction path of silver ions towards preexisting surfaces (bottom) [6].4
- Figure 2. 2 (a) Schematic drawing of diameter change with AgNO_3 concentration [9] (b) diameter (left) and length (right) change with respect to PVP: AgNO_3 ratio [10].6
- Figure 2. 3 (a) Schematic illustration of effect of PVP concentration on dimensions of Ag NWs [13], (b) on shape of final products [14].8
- Figure 2. 4 (a) Length distribution of Ag NWs with 0.19 mM(left) and 0.36 mM (right) CuCl_2 (b) Diameter distribution of Ag NWs with 0.19 mM and 0.36 mM CuCl_2 and without CuCl_2 [15].....9
- Figure 2. 5 (a) Schematic illustration of galvanic replacement and conformal deposition routes [26], (b) A TEM image of Ag-Au core-shell NW [27], (c) Change the Pt layer thickness with time (inset shows decrease in diameter of Ag NWs) [28].13
- Figure 2. 6 (a) Time dependent thickness change of MoO_2 shell layer (inset shows a SEM image) during electrodeposition, [30] (b) Schematic illustration of routes for conformal or bristled TiO_2 coating on Ag NWs, [31] (c) concentration change of MB with time [37].14
- Figure 2. 7 Schematic illustrations and SEM images of pristine Ag NWs and Ag NWs-PEDOT:PSS composite [38].15
- Figure 2. 8 (a) Time dependent sheet resistance change for pristine Ag NWs and Ag NWs-graphene hybrid electrodes, (b) Temperature profiles for pristine Ag NWs and Ag NWs-graphene hybrid (annealed at different temperatures) electrodes and (c) temperature profile for Ag NWs-graphene hybrid electrodes under different applied

potentials [44]. (d) Ammonia responses of Ag NWs, SWCNT and Ag NWs-SWCNT sensors and (e) ammonia response of SWCNT with various Ag NWs amounts [39].	17
.....	17
Figure 2. 9 Photographs showing the color change during the polyol synthesis of Ag NWs after (a) 1 min (b) 40 min and (c) 80 min.....	19
Figure 2. 10 (a) HR-TEM image (b) SEM image (c) Diameters distribution and (d) XRD pattern of purified Ag NWs synthesized via polyol method. (JCPDS Card no: 04-0483).....	23
Figure 2. 11 (a) SEM and (b) TEM images and (c) diameter distribution of Ag-Pt core-shell NW networks using 0.95 ml of 0.01 M chloroplatinic acid solution.....	24
Figure 2. 12 (a) TEM image of Ag-Pt core-shell NWs, EDS mapping for (b) Ag, (c) Pt (d) EDS line mapping for Ag and Pt and (e) line profile for red line in part (d). (dark blue lines for Ag and light blue lines for Pt).....	25
Figure 2. 13 (a) SEM image of Ag-Pt core-shell NWs, EDS mapping for (b) Ag and (c) Pt.....	25
Figure 2. 14 (a) SEM image (inset shows a low magnification SEM image) and (b) diameter distribution of Ag-Pt core-shell NWs synthesized using 0.71 ml of 0.01 M chloroplatinic acid.	26
Figure 2. 15 (a) SEM image of Ag-Pt core-shell NWs synthesized using 0.71 ml of 0.01 M chloroplatinic acid. EDS maps for (b) Ag and (c) Pt.	26
Figure 2. 16 (a) (a) SEM image (inset shows low magnification SEM image) and (b) diameter distribution of Ag-Pt core-shell NWs with 0.47ml of 0.01 M chloroplatinic acid.....	27
Figure 2. 17 (a) TEM image of Ag-Pt core-shell NWs synthesized using 0.47 ml of 0.01 M chloroplatinic acid. EDS map for (b) Ag and (c) Pt, (d) EDS line map for Ag and Pt and (e) Line profile for red line in part (d). (dark green lines for Ag and light blue lines for Pt in part (b), (c), (d) and(e)) (f) SEM image of Ag-Pt core-shell NWs. EDS maps for (g) Ag and (h) Pt. XPS curve fitting for (i) Ag and (j) Pt.	29

Figure 2. 18 (a) SEM images of Ag-Pt Core-Shell NWs synthesized using 0.1 ml of 0.01 M chloroplatinic acid. (inset shows low magnification SEM image). (b) SEM image used for EDS areal mapping. EDS maps for (c) Ag and (d) Pt.	30
Figure 2. 19 SEM image of Ag NWs exposed to AA-PVP solution.	32
Figure 2. 20 SEM image of Ag-Pt core-shell NWs synthesized in a reaction medium with a pH value of 8.0 (inset shows low magnification SEM image).	33
Figure 2. 21 SEM image of Ag-Pt core-shell NWs synthesized in a reaction medium with a pH value of 4.0.	34
Figure 2. 22 SEM image of Ag-Pt core-shell NWs where DEHA-Ag NWs suspension was used.	35
Figure 2. 23 SEM image of Ag-Pt core-shell NWs synthesized in an ice bath.	36
Figure 2. 24 SEM images of Ag-Pt core-shell NWs s with injection of (a) 0.48 mM, (b) 3.93 mM and (c) 9.53 mM chloroplatinic acid solution.	37
Figure 3. 1 (a) Schematic of measurement setup, (b) CV results of bare Ag NW electrode and (c) CV results of Ag-Au core-shell NW electrode [27].	40
Figure 3. 2 CV results of Ag-Au-PPy core-shell NWs (a) at different scan rates, (b)) different PPy thickness.(c) Galvanostatic charge discharge results for Ag-Au-PPy core-shell NWs with different PPy thicknesses [48].	41
Figure 3. 3 (a) CV results of Ni(OH) ₂ - Ag core-shell NWs at different coating times and (b) different scan rates [49].	41
Figure 3. 4 Resistance change with time nder 85 %RH at 85 °C.	42
Figure 3. 5 (a) Resistance chance with exposure of H ₂ O ₂ solution time [27], (b) TEM images of Ag NW and Ag-Au core-shell NWs after exposure H ₂ O ₂ solution (Scales are 1 μm) and (c) UV-Vis spectra of Ag NWs and Ag-Au core-shell NWs before/after exposure H ₂ O ₂ solution [51].	43
Figure 3. 6 (a)Schematic illustration and SEM images of Ag NWs and coated Ag NWs annealed at 300 for 5 min (b) Resistance chance with temperature for Ag NWs with average diameters of 17, 45 and 120 nm [53].	44
Figure 3. 7 (a) Resistance change with time for 150 °C, (b) 75 °C and (c) room temperature (black lines for bare Ag, red lines for Ag-Pt).	47

Figure 3. 8 SEM images of electrodes after 150 °C measurement (a) for Ag-Pt core shell NWs and (b) for bare Ag NWs. SEM images of electrodes after 75 °C measurement (a) for Ag-Pt core shell NWs and (b) for bare Ag NWs.....	48
Figure 3. 9 (a) Resistance change with time for 85 %RH , (b) 75 %RH and (c) 43 %RH (black lines for bare Ag, red lines for Ag-Pt).	49
Figure 3. 10 SEM images of electrodes kept in 85% RH (a) for Ag-Pt core shell NWs and (b) for bare Ag NWs, 75 %RH level (c) for Ag-Pt core shell NWs and (d) for bare Ag NWs.	50
Figure 3. 11 (a) Resistance change with time for H ₂ O ₂ stability measurement (black line for bare Ag, red line for Ag-Pt) (inside is early stage of the measurement), SEM images of electrodes after H ₂ O ₂ treatment (b) for Ag-Pt core shell NWs and (c) for bare Ag NWs (black line for bare Ag, red line for Ag-Pt).	51
Figure 3. 12 The electrochemical stability of bare Ag NWs (first and second cycles) compared with Ag-Pt core-shell NW networks by applying 0.0-0.9 V.....	52
Figure 3. 13 The CVs of Ag-Pt core-shell NWs network under applying different potential windows.....	53
Figure 4. 1 Optical transmittance with respect to areal mass density of Ag NWs with different diameters [78].	56
Figure 4. 2 Thermal response of Ag NW networks (inset shows the derivative curve to obtain the heating and cooling rates) [68].	58
Figure 4. 3 Heating/cooling curve for bare Ag NWs and AZO coated Ag NWs applied potential of (a) 2.25 and (b) for 3 V/cm (inset show SEM image of AZO coated Ag NWs) [72].	59
Figure 4. 4 (a) Thermal performance of Ag NWs, Ag NF networks and ITO heaters. (b) Heating/cooling curves during stepwise increase in voltage from 0.5 to 4.5 V. (c) Thermal camera images of Ag NF electrode under different voltages [82].	59
Figure 4. 5 Thermal performance of wearable Ag NWs/PVA film and in-situ temperature measurements [83].	60
Figure 4. 6 (a) Stepwise heating curve and (b) thermal camera images of stepwise heated Ag-Pt core-shell NW electrodes.....	62

Figure 4. 7 Stepwise heating and cooling of Ag-Pt core-shell NW electrodes (inset shows SEM image of electrode after the measurement).....63

LIST OF ABBREVIATIONS

ABBREVIATIONS

AA	Ascorbic Acid
AAO	Anodized Aluminum Oxide
Ag	Silver
Ag NFs	Silver Nanofibers
Ag NPs	Silver Nanoparticles
Ag NWs	Silver Nanowires
AgCl	Silver Chloride
AgNO ₃	Silver Nitrate
ALD	Atomic Layer Deposition
Au	Gold
AZO	Aluminum Doped Zinc Oxide
CNT	Carbon Nanotube
Cu NWs	Copper Nanowires
CuCl ₂	Cupric Chloride
CV	Cyclic Voltammetry
CVD	Chemical Vapor Deposition
DEHA	Diethylhydroxylamine
DEZ	Diethylzinc
DI	Deionized
DNA	Desoxyribonucleic Acid
EDLC	Electrochemical Double Layer Capacitance
EDS	Energy Dispersive Spectrometry
EDX	Energy Dispersive X-Ray Analysis
EG	Ethylene Glycol
FeCl ₃	Iron(III) Chloride
H ₂ O	Water
H ₂ O ₂	Hydrogen Peroxide
H ₂ PtCl ₆	Chloroplatinic Acid
H ₃ PO ₄	Phosphoric acid
HAuCl ₄	Chloroauric Acid
HR-TEM	High-resolution Transmission Electron Microscopy
ITO	Indium Tin Oxide
KBr	Potassium Bromide
LiClO ₄	Lithium Perchlorate

MB	Methylene Blue
MnO ₂	Manganese Dioxide
Na ₂ MoO ₄	Sodium Molybdate
Na ₂ Pt(OH) ₆	Sodium Hexahydroxyplatinate(IV)
Na ₂ SO ₄	Sodium Sulfate
NaCl	Sodium Chloride
NaOH	Sodium Hydroxide
NH ₄ OH	Ammonium Hydroxide
Ni	Nickel
Ni(OH) ₂	Nickel(II) Hydroxide
PC	Propylene Carbonate
Pd	Paladium
PET	Polyethylene Terephthalate
PMMA	Poly(methyl methacrylate)
PPy	Polypyrrole
Pt	Platinum
PVA	Polyvinyl Alcohol
PVP	Poly(vinylpyrrolidinone)
RH	Relative Humidity
SEM	Scanning Electron Microscopy
SERS	Surface Enhanced Raman Scattering
Si	Silicon
SiO ₂	Silicon Dioxide
STEM	Scanning Transmission Electron Microscopy
TEM	Transmission Electron Microscopy
THF	Thin Film Heater
UV	Ultraviolet
XPS	X-Ray Photoelectron Spectroscopy
XRD	X-Ray Diffraction
ZnO	Zinc Oxide

LIST OF SYMBOLS

SYMBOLS

μm	micrometer
Ω	ohm
θ	theta
$^{\circ}$	degree
ϵ_r	Dielectric constant of dielectric material
ϵ_0	Dielectric constant of vacuum
σ	Stefan-Boltzmann constant
α	Thermal expansion coefficient

CHAPTER 1

INTRODUCTION

Technological demand started with the human history in order to overcome the problems that are encountered in the daily life. Once there was a need for stone and wooden tools, now there is a need for computers, electric vehicles and much more. Therefore, shaped by such demands, there exists huge and rapid development in technology. Nowadays, flexible, transparent and stretchable electronic devices are receiving significant attention by both scientific and industrial communities due to their necessity in photovoltaics, energy storage devices like supercapacitors and batteries, heaters, light emitting diodes (LEDs), and touch screens. Many different kinds of materials have developed to meet and enhance the requirements of these applications. Most common examples of these materials are thin films of indium tin oxide (ITO), fluorine doped tin oxide (FTO), aluminum doped zinc oxide (AZO), carbon nanotubes (CNTs), graphene, poly(3,4-ethylenedioxythiophene)-poly(styrenesulfonate) (PEDOT:PSS), polypyrrole (PPy), metal nanostructure networks and metal nanowires. Most widely investigated metal nanowires include gold, silver and copper nanowires. Among them, silver nanowires (Ag NWs) are the first to be reproducibly synthesized in large quantities. Ag NWs can be deposited onto various substrates to form percolation, random networks. The optoelectronic properties of Ag NW networks are comparable or even better than those of the current transparent conducting materials.

This work discloses a novel method for the enhancement of the electrochemical, chemical and environmental stabilities of Ag NW networks. This is achieved through electroless deposition of a conformal platinum shell layer on Ag NWs. Following the deposition of the Ag-Pt core-shell NW networks, their electrochemical, chemical and environmental stabilities were compared to that of bare Ag NW networks.

This thesis contains 3 chapters. Chapter 2 emphasizes to the selected polyol synthesis method. Advantages and disadvantages of synthesis methods are discussed. Detailed microstructural characterization of the Ag NWs synthesized through polyol synthesis is also discussed. This chapter also describes the synthesis of Ag-Pt core-shell NWs through electroless Pt deposition and following the discussion were made in the light of the literature. A detailed parametric study on Pt deposition was conducted, which was followed by a detailed material characterization of Ag-Pt core-shell NWs. Characterization routes include transmission electron microscope (TEM), energy dispersive X-ray spectroscopy (EDS) and X-ray photoelectron spectroscopy (XPS). In the fourth chapter, environmental, chemical and electrochemical stabilities of the Ag-Pt core-shell NW networks are investigated and compared to that of bare Ag NW networks. In all comparison tests, superior performance of Ag-Pt core-shell NW network on that of bare Ag NW network are achieved. Lastly, Chapter 4 deals with the characterizations of Ag-Pt core-shell NW networks based thin film heaters. The performance of thin film heaters is monitored using both a thermocouple and a thermal camera.

CHAPTER 2

SILVER PLATINUM CORE SHELL NANOWIRES

2.1. Synthesis of Ag NWs

During the past years, the need for synthesis of the nanostructures have expanded in various fields such as photovoltaics, light emitting diodes and energy storage devices [1]. Researchers have developed numerous methods to obtain the desired nanostructures using both physical and chemical routes [2]. Although the physical methods such as supersonic airflow pulverization can be used for production of nanostructures, chemical methods are more versatile in the synthesis of them [3]. The chemical methods for Ag NWs are more preferred due to easiness of the process control, ability of mass production and low cost [2]. The chemical methods involve ultraviolet irradiation, template (solvothermal) and polyol method. In this thesis, the improved polyol method was followed to synthesize Ag NWs for further use.

2.1.1. Polyol Method

The polyol method is a solution based synthesis method, where the solvent acts both as the solvent for the precursor and the reducing agent during the reaction [4]. The polyol method is the most successful synthesis route and has clear advantages such as low cost, large-scale synthesis of single crystalline Ag NWs and simple control of parameters over the other synthesis methods. The Ag NWs synthesis based on polyol method was reported by Sun et al. [5] for the first time in late 2001. He and his co-workers developed a method in which PtCl_2 was dissolved in EG and reduced at 160 °C to form platinum nanoparticles acting as seeds and then a solution of AgNO_3 -PVP was added onto Pt seed solution. Afterwards, reaction was continued at 160 °C for 60 min and the synthesized Ag NWs had diameters of 30-40 nm and lengths of 50 μm on average. Thus the aspect ratio of the nanowires were about 1000. A SEM image of the

synthesized Ag NWs from this work is given in Figure 2. 1 (a). Following this first publication, the next study was published by Sun et al. [6] clarified the growth mechanism of Ag NWs, morphology of Ag NWs, surface planes of Ag NWs and the role of PVP. The results can be summarized as follow;

1. Ag NWs have five folded twinned crystal structure with pentagonal morphology,
2. The side surfaces of Ag NWs are determined as $\{100\}$ planes while, the end surfaces of Ag NWs are $\{111\}$ planes of Ag crystal,
3. PVP completely covers the $\{100\}$ planes of the Ag NWs and seeds formed in the early stage of synthesis, in other words, $\{100\}$ surfaces of Ag are passivated by PVP. Besides, PVP attaches to $\{100\}$ planes of the Ag NWs to a certain degree. Moreover, with the help of PVP, seeds get larger in size Ostwald ripening, which is defined as the dissolution of small nuclei into solution and at the same time, enlargement of big nuclei [7],
4. The anisotropic growth proceeds in longitudinal direction since PVP blocks the $\{100\}$ surfaces. Therefore, seeds grow in $\langle 110 \rangle$ direction of Ag crystal.

Figure 2. 1 (b) shows a schematic drawing of the Ag NW growth mechanism (top) and reduction path of Ag ions towards preexisting surfaces (bottom).

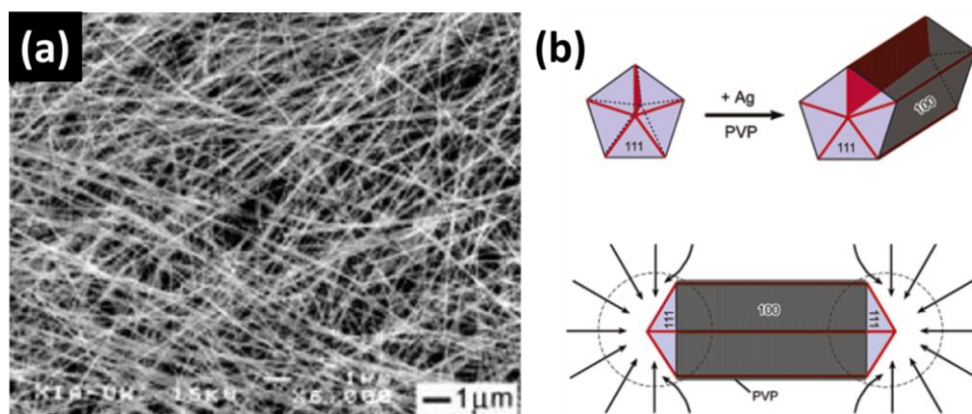


Figure 2. 1 (a) SEM image of Ag NWs synthesized by polyol method for the first time [5] (b) Schematic drawings of growth mechanism of Ag NWs; penta-twinned Ag NWs formation from nanorod (top) and reduction path of silver ions towards preexisting surfaces (bottom) [6].

As being the most promising method to synthesize Ag NWs, the polyol method has been studied extensively to further optimize the experimental parameters and mass-production. In this chapter, experimental parameters of the polyol method are examined in detail. Parameters include effects of AgNO₃, PVP, metal salts addition, reaction temperature and other parameters like stirring rate and injection time.

Before going into details of synthesis parameters, it is necessary to state what reagents are required in the reaction medium to synthesize Ag NWs via the polyol method. First of all, a polyol which gives the name to the method is essential during the reaction to reduce the Ag⁺ ions to metallic Ag. For Ag NW synthesis, ethylene glycol (EG) is the most favored polyol due to its high boiling point (196 °C) and dissolving ability of both AgNO₃ and PVP. Secondly, a Ag source is required to supply ions to the reaction medium and AgNO₃ salt is a preferred source due to its low cost and availability. Thirdly, a capping agent is a fundamental constituent to achieve one dimensional growth of Ag NWs and polyvinylpyrrolidone (PVP) is used as the capping agent. Besides these three essential reagents, some salts are added to control the final morphology of Ag NWs and to increase the synthesis yield [8].

2.1.1.1. Effect of Silver Nitrate Concentration

AgNO₃ has a very important role as the silver source during the synthesis as stated before. The morphology of Ag NWs, aspect ratio of Ag NWs and yield of the synthesis can be controlled by adjusting the concentration or injection rate of the AgNO₃. In the literature, there are two ways to study the influence of AgNO₃ such that concentration of AgNO₃ is varied while the concentration of PVP is kept constant and concentrations of both AgNO₃ and PVP are changed while keeping the AgNO₃:PVP ratio constant. The effect of the concentration of AgNO₃ on the aspect ratio of the Ag NWs was examined by Lin et al. [9] in the polyol method. In this study, the effect of AgNO₃ concentration was investigated under constant PVP. It was found that Ag NWs with high aspect ratio can be synthesized at low AgNO₃ concentrations. Figure 2. 2 (a) schematically shows the change in diameters of Ag NWs with the AgNO₃

concentration. Coskun et al. [10] revealed the relationship between the molar ratio of PVP:AgNO₃ and the final diameter and length of NWs. Figure 2. 2 (b) shows the decrease in diameter (left) and length (right) with increase in the PVP: AgNO₃ ratio. The results showed that the diameters of Ag NWs decreased from 300 nm to 50 nm and the lengths of Ag NWs was decreased from 17 μm to 5 μm upon increasing the PVP: AgNO₃ ratio.

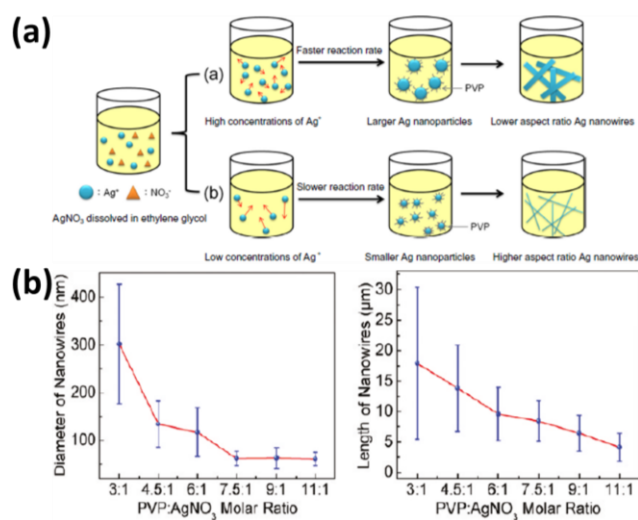


Figure 2. 2 (a) Schematic drawing of diameter change with AgNO₃ concentration [9] (b) diameter (left) and length (right) change with respect to PVP:AgNO₃ ratio [10].

Nekahi et al. [11] proved the importance of the concentration of AgNO₃ in enhancing the yield of the polyol synthesis of Ag NWs. In this study, synthesis was carried out with different concentrations of AgNO₃ as 0.07 M, 0.085 M and 0.1 M while other parameters were kept constant. The syntheses with a AgNO₃ concentration of 0.07 M and 0.1 M yielded low amount of Ag NWs and formation of large amounts of Ag NPs occurred. In addition to low efficiency, when the AgNO₃ concentration was increased to 0.1 M, the lengths of Ag NWs also decreased. However, when the polyol synthesis was carried using the concentration of 0.085 M of AgNO₃, yield of the synthesis reached to 95%. Yield was determined as the ratio of synthesized Ag NWs to the final synthesis products.

2.1.1.2. Effect of Polyvinylpyrrolidone (PVP) Concentration

PVP is a crucial component for the polyol synthesis of Ag NWs because of its chemical structure and properties. PVP has long molecular chains which wrap the surface of silver nanomaterials, in this case nanowires, to avoid agglomeration. Moreover, PVP has an affinity with certain crystallographic planes of Ag seeds to lead to the formation of one-dimensional structures [2][12]. Therefore, there are many publications that investigate the amount of PVP on the morphology of the final Ag NWs.

Lin et al. [13] found the effects of the molecular weight of PVP and the concentration of PVP on the morphology of the synthesized products. In this work, polyol synthesis was conducted using PVP with molecular weights of 40K g/mol and 360K g/mol and the ratio of PVP:AgNO₃ was varied between 0.5, 1.5 and 2.5. Ag NPs were formed using 40 K PVP at all different molar ratios. On the other hand, when 360 K PVP was used in the synthesis, Ag NWs with average diameters of 170 nm and lengths of 10 μm were synthesized at a PVP: AgNO₃ ratio of 2.5. Moreover, it was also found that the aspect ratio of Ag NWs decreased gradually and Ag NPs grown when the ratio of PVP:AgNO₃ reduced to 1.5 and 0.5. Figure 2. 3 (a) schematically illustrates the effect of PVP concentration on the dimensions of Ag NWs.

In addition to Lin's findings, Yang et al. [14] performed a series of experiments to reveal the effects of PVP on the polyol method. In the experiments, the effect of different molecular weights of PVP, 24 K, 45-55 K, 58 K and 130 K g/mol on the synthesis products were investigated and results showed that the length of the final Ag NWs increased when PVP with higher molecular weight was used. Another result showed that the length of Ag NWs increased but the diameter of Ag NWs was found to decrease when the ratio of PVP:AgNO₃ was increased from 3.0 to 5.0, which supported the Lin's study. Lastly, in the absence of PVP in the reaction medium, Ag NPs form rather than the formation of the Ag NWs. Figure 2. 3 (b) schematically illustrates the final products of polyol synthesis with and without PVP.

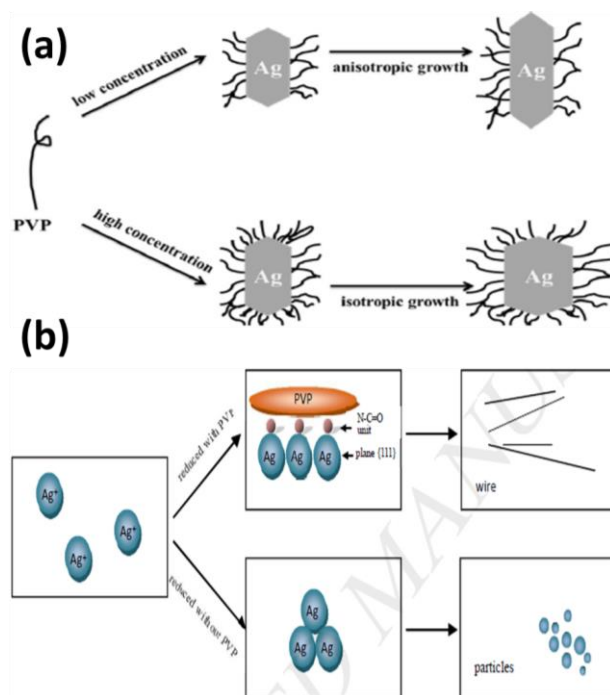


Figure 2. 3 (a) Schematic illustration of effect of PVP concentration on dimensions of Ag NWs [13], (b) on shape of final products [14].

2.1.1.3. Effect of Metal Salts

In addition to the effect of AgNO_3 and PVP on the polyol synthesis, addition of metal salts play an important role on the yield and morphology of Ag NWs. This is because the metal salts provide ions into the reaction medium. In this regard, several salts have been involved in the reactions and common examples include sodium chloride (NaCl), potassium bromide (KBr), cupric chloride (CuCl_2) and iron(III) chloride (FeCl_3).

The effects of the Cu^{2+} concentration on the morphology of Ag NWs was investigated by Wang et al.[15] with the addition of CuCl_2 into the reaction. In the polyol method, 0.19 mM and 0.36 mM of CuCl_2 were dissolved in EG then, the AgNO_3 and PVP were injected into this solution. The average lengths of the synthesized NWs were $8.2 \pm 3.7 \mu\text{m}$, $12.6 \pm 6.6 \mu\text{m}$ and $49.4 \pm 24 \mu\text{m}$ for without CuCl_2 , 0.19 mM CuCl_2 and 0.36 mM CuCl_2 , respectively. Synthesized Ag NWs had the corresponding average diameters of $48 \pm 7 \text{ nm}$, $49 \pm 14 \text{ nm}$ and $72 \pm 13 \text{ nm}$ for the cases without CuCl_2 , 0.19 mM CuCl_2 and 0.36 mM CuCl_2 , respectively. Therefore, it was concluded that

increasing the Cu^{2+} concentration in the reaction medium increased both the average length and the diameter of Ag NWs. Figure 2. 4 (a) and (b) show the length and diameter distributions of the synthesized Ag NWs with different CuCl_2 concentrations, respectively. In addition to the changes in the morphology of Ag NWs, the addition of CuCl_2 also enhanced the reaction kinetics by increasing the adsorption rate of Ag atoms. Thus, the total polyol synthesis took about 30 min, where, the synthesis time was 90 min in absence of Cu^{2+} ions in the reaction. Similar results were obtained by the Chen et al. [16]. Presence of FeCl_3 in the reaction medium was also investigated and the uniformity and crystallinity of Ag NWs synthesized with FeCl_3 was compared to those synthesized with CuCl_2 . The experiments were conducted with the same amount of Cl^- ions in the reaction medium and results showed that both CuCl_2 and FeCl_3 were effective in achieving NWs with higher uniformity and crystallinity. However, it was also stated that Fe^{3+} ions were more dominant than Cu^{2+} ions in increasing the length of NWs.

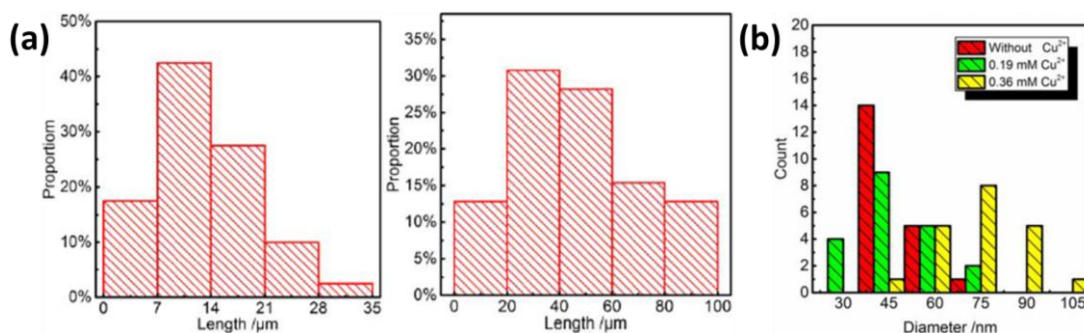


Figure 2. 4 (a) Length distribution of Ag NWs with 0.19 mM(left) and 0.36 mM (right) CuCl_2 (b) Diameter distribution of Ag NWs with 0.19 mM and 0.36 mM CuCl_2 and without CuCl_2 [15]

The effects of sodium chloride (NaCl) on the polyol synthesis have been studied by many research groups. First of all, formation of the initial Ag seeds is controlled by the concentrations of Ag^+ and Cl^- ions, which form AgCl compound. When there is excess amount of Cl^- ions, the formation of silver chloride (AgCl) compound take place and the number of Ag seeds decreases. Therefore, as the possible nucleation sides for Ag^+ ions decreases, the synthesis results in longer NWs [17]. In other studies, it was found that the efficiency of the polyol synthesis was enhanced with the addition

of NaCl since there would be less number of Ag nanoparticles (NPs) in the presence of NaCl [18], [19]. Moreover, similar results are obtained for the synthesis with the addition of KBr rather than NaCl. It was found that the aspect ratio of Ag NWs increased together with the synthesis efficiency upon KBr addition [19], [20].

2.2. Coating of Nanowires

Metallic materials are generally prone to corrode under ambient conditions due to their thermodynamic and kinetic instability [21]. They have higher Gibbs free energies than their other forms such as oxides, sulfides and hydrates. In the case of silver, surface of bulk tarnishes because the formation of silver sulfide (Ag_2S) compound is favorable although silver is known to be corrosion resistant [22]. During the corrosion of silver, the formations of silver chloride (AgCl) and silver oxide (Ag_2O) are also possible depending on the environmental conditions [23]. Thus, special methods like alloying, coating and surface treatments are used to extend the service life of Ag [24].

These instabilities increase drastically when the size of the metallic materials decreases from bulk to nanometer size. Therefore, it is crucial to develop methods that protect the nanomaterials from the corrosion when they are used in applications.

There are many Ag based nanomaterials. Common examples are nanospheres, nanocubes, triangular nanoplates, nanorods, nanoparticles (NPs) and NWs. Among them, Ag NWs have attracted a huge attention due to its excellent optical, electrical and thermal properties in conjunction with the biocompatibility of Ag. Moreover, percolative networks of Ag NWs have a potential to replace the commercially available transparent and conductive materials since synthesis of Ag NWs, their deposition onto various substrates and integration in applications are very flexible, scalable and cost-effective compared to those commercial materials. However, as the nature of being a nanomaterial, Ag NWs suffer from corrosion, commonly sulfidation and oxidation, in different environments. As an example, Ag NW percolative networks were left in ambient conditions and the structural changes were monitored by Elechiguerra et al. It was found that a 15 nm thick film of Ag_2S formed along the

Ag NWs surface on fourth week and the percolating network completely destroyed in six months after fabrication [25]. Therefore, considering this corrosion behavior of Ag NWs, fabrication of composite structures has been studied extensively with Ag NWs and different kinds of materials to improve the service life of the percolative networks of Ag NWs. Moreover, the composite component combined with Ag NWs can be metals, oxides/sulfides/hydrates, polymers and carbon based materials. This kind of composites containing Ag NWs are named as core-shell, core-sheath, coaxial or hybrid nanowires/nanostructures in the literature. In this chapter, the core-shell terminology will be used to refer to Ag NWs and coating material, respectively.

2.2.1. Metal Coating

Ag NWs were coated with various metals like gold (Au), platinum (Pt), palladium (Pd) and nickel (Ni) to manipulate the surface properties of them and enhance the network properties in terms of electrochemical stability, environmental stability, chemical stability and biocompatibility compared to that of bare Ag NWs.

Before going into the results from literature about core-shell nanowires, it is very important to mention about the study done by Yang et al. [26]. The optimum experimental conditions were reported to deposit conformal and thin (0.6 nm) Au layer on Ag nanocubes. The roles of constituents in the reaction medium were determined such that ascorbic acid (AA) acted as reducing agent for gold (III) chloride trihydrate (HAuCl_4) and polyvinylpyrrolidone (PVP) acted as capping agent and stabilizer. In Figure 2. 5 (a), it was revealed that a conformal coating and galvanic replacement took place according to which route was followed through the process. In the case of the reaction rate of galvanic replacement was higher than that of reduction of AA, galvanic replacement between HAuCl_4 and Ag was observed. On the other hand, when the reaction rate of galvanic replacement was lower than that of reduction of AA, conformal Au coating on Ag nanocubes occurred. The synthesized Ag-Au core-shell nanocubes were compared with pristine Ag nanocubes in terms of chemical stability and surface-enhanced Raman scattering response. When both were exposed to a 2.3%

hydrogen peroxide (H_2O_2) solution, Ag-Au core-shell nanocubes did not oxidize for 10 h but the pristine Ag nanocubes were found to dissolve only after 3 mins.

Ag-Au core-shell NWs synthesis was reported by Lee et al. [27] via the wet chemical route. The synthesis was conducted in such a way that AA-PVP- sodium hydroxide (NaOH) solution was prepared and Ag NWs-DI water dispersion was added into that solution. After the addition was completed, dilute HAuCl_4 solution was injected using a syringe pump with very slow rate. Using the described route, Ag NWs with 30 nm diameter were coated with 5 nm a thick Au layer. A TEM image of Ag-Au core-shell NWs is provided in Figure 2. 5 (b). The results revealed that electrode with Ag-Au core-shell NWs synthesized with this route had comparable sheet resistance, transparency and stretchability to that of the pristine Ag NWs. Stability under ambient conditions and exposure of H_2O_2 solution were also compared. Ag NWs networks were found to fail after 30 days under ambient conditions. It was also observed when it was subjected to H_2O_2 solution, Ag NW networks failed only after a few seconds. On the other hand, Ag-Au core-shell NW networks were still functional under those conditions. Moreover, electrochemical stability of NWs network was enhanced with Au coating. For pristine Ag NW networks, after the first measurement cycle, irreversible oxidation of Ag occurred at a potential of 0.45 V and the network was found to get destroyed. On the other hand, Ag-Au core-shell NW networks continued to operate even after 50 cycles in a widened (0-0.6 V) potential window.

Ag-Pt core-shell NWs have been studied only in a limited number of publications. A study on kinetics of nanocrystalline Pt deposition on Ag NWs was done by Shen et al. [28]. In this work, Ag NWs were grown on Si template via thermally assisted photoreduction. Pt deposition was performed using sodium hexahydroxyplatinate(IV) ($\text{Na}_2\text{Pt}(\text{OH})_6$) solution. $\text{Na}_2\text{Pt}(\text{OH})_6$ solution and Ag NWs were isothermally heated at three different temperatures (100, 170 and 200 °C) and deposition of Pt nanocrystals were examined. Results showed that high reduction potential of Pt ions can be reduced by the oxidation of Ag atoms and kinetics of the Pt deposition was found to depend

on the reaction between Pt and Ag ions. Therefore, as the diameter of Ag NWs decreased, Pt shell layer thickened, shown in Figure 2. 5 (c).

Other than Ag-Pt core-shell NWs, solution based synthesis of Cu-Pt core-shell NWs were also studied [29]. Reaction medium containing AA, PVP, Cu NWs, DEHA and K_2PtCl_6 was prepared to deposit a 50 nm thick Pt shell layer on Cu NWs. Following the deposition, oxidation behavior of Cu-Pt core-shell NW networks was examined under different temperatures and CV potentials between -1.0 and 0.2 V. Enhanced performance of core-shell NWs over pristine NWs was reported.

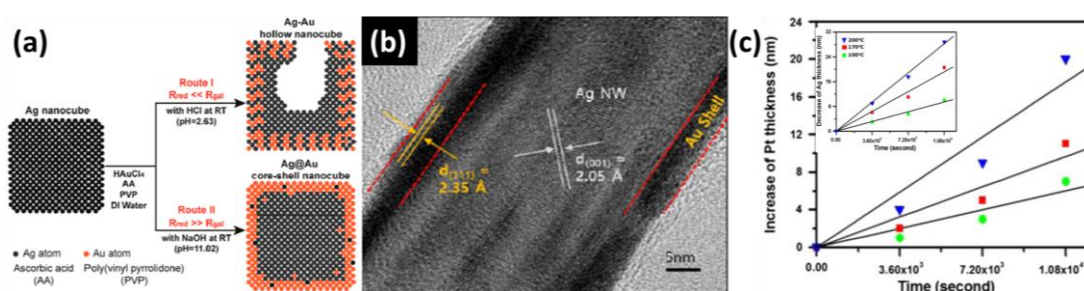


Figure 2. 5 (a) Schematic illustration of galvanic replacement and conformal deposition routes [26], (b) A TEM image of Ag-Au core-shell NW [27], (c) Change the Pt layer thickness with time (inset shows decrease in diameter of Ag NWs) [28].

2.2.2. Oxide Coating

Ag NWs were coated with various oxide materials such as MoO_2 [30], TiO_2 [31]–[33], ZnO [34], Cu_2O [35] and SiO_2 [36] via different synthesis routes. MoO_2 shell layer on Ag NWs was deposited via electrochemical route using 0.1 M sodium molybdate (Na_2MoO_4) solution by applying a constant potential of -1.2 V. Thickness of the coated shell layer was measured as 50-250 nm for 200-1600 seconds of deposition time, as shown in Figure 2. 6 (a). A conformal coating was achieved. Although MoO_2 was chemically stable and had different valance states, which provided pseudocapacitive property, it had low electrical conductivity. As stated before, Ag NWs had high electrical conductivity. Therefore, low electrical conductivity of MoO_2 was enhanced via the fabrication of Ag NWs- MoO_2 core-shell NW networks. The Ag NW- MoO_2 core-shell NW networks were used as supercapacitor electrodes and the

capacitance of it was measured as 500 F/g, which was higher value than that of porous MoO₂ (146 F/g).

TiO₂ was deposited on to Ag NWs via a solution based method. Du et. al [31] reported that TiO₂ with different morphologies can be deposited onto Ag NWs in EG as schematically shown in Figure 2. 6 (b). Ag-TiO₂ core-shell NWs, with a core diameter of 40 nm and a shell thickness of 35 nm were synthesized at temperatures of 240 and 270 °C, respectively to obtain conformal or bristled coating. On the other hand, deposition of TiO₂ via sol-gel on Ag NWs was reported by Chin et al. [32]. A 10 nm of TiO₂ shell was coated onto Ag NWs with a diameter of 70 nm and the synthesized Ag-TiO₂ core-shell NWs were utilized in a photocatalytic application. Decomposition of methylene blue (MB) was monitored both in the presence and absence of Ag-TiO₂ core-shell NWs with and without UV light irradiation, results of which are provided in Figure 2. 6 (c). Change in concentration of MB did not occur for 3 cases; Ag-TiO₂ and MB without UV light irradiation, pristine Ag NWs-MB with UV light irradiation and MB with UV light irradiation. However, when 5 and 10 mg of Ag-TiO₂ core-shell NWs were mixed with MB, decomposition of MB was observed under UV light irradiation. Moreover, upon doubling the amount of Ag-TiO₂ core-shell NWs, the rate of MB decomposition was found to increase twice.

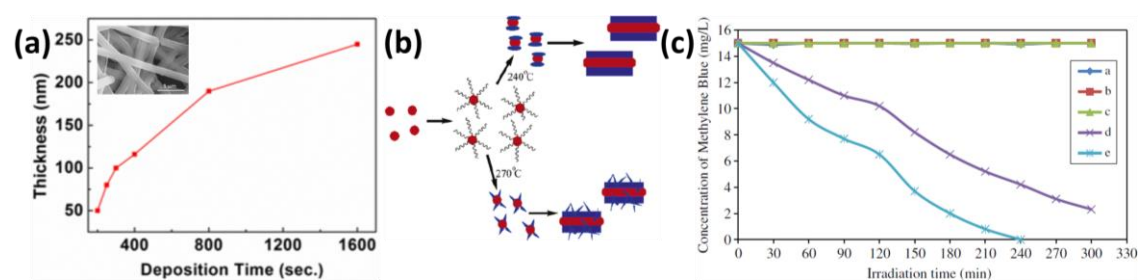


Figure 2. 6 (a) Time dependent thickness change of MoO₂ shell layer (inset shows a SEM image) during electrodeposition, [30] (b) Schematic illustration of routes for conformal or bristled TiO₂ coating on Ag NWs, [31] (c) concentration change of MB with time [37].

2.2.3. Polymer Coating

Ag NW networks have been coated with poly(3,4-ethylenedioxy thiophene) polystyrene sulfonate (PEDOT:PSS), which is a conducting transparent polymer. The

reason for PEDOT:PSS coating coated is that it protects the Ag NWs from corrosion and preserve high conductivity of Ag NW networks. Morphology of the PEDOT:PSS coated Ag NWs appears such that Ag NWs are embedded inside the polymer.

Choi et al. [38] reported two step spray coating of Ag NWs and PEDOT:PSS. The roughness and the contact resistance of pristine Ag NWs and Ag NWs-PEDOT:PSS composite networks were compared (Figure 2. 7). The results showed that roughness of Ag NWs-PEDOT:PSS composite networks was smaller than that of pristine Ag NW networks since PEDOT:PSS applied a force on Ag NWs to be bent towards the substrate. When 100 nm thick PEDOT:PSS was coated onto Ag NW networks, the root-mean-square roughness value decreased from 300 nm to 51.8 nm. In addition to roughness, the contact resistance of the Ag NWs decreased after deposition of PEDOT:PSS due to the increase in the contact area of Ag NWs with each other and the conductive nature of the PEDOT:PSS.

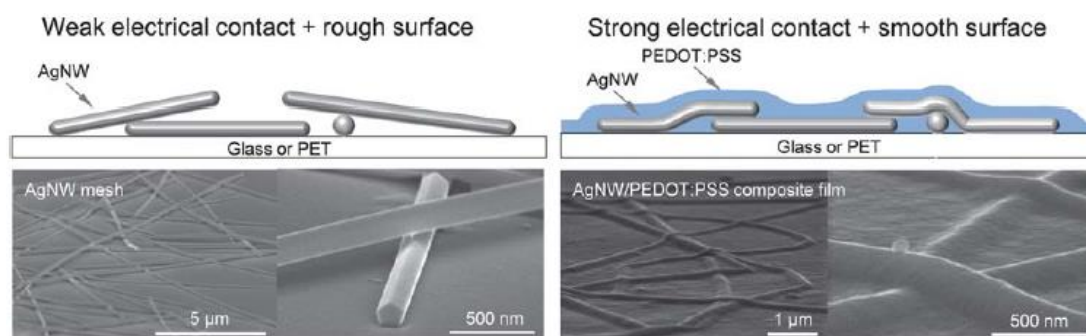


Figure 2. 7 Schematic illustrations and SEM images of pristine Ag NWs and Ag NWs-PEDOT:PSS composite [38].

2.2.4. Hybrid Structures with Carbon-Based Materials

Ag NWs are combined with carbon based materials to form hybrid conductive transparent electrodes. The most common examples of carbon based materials are carbon nanotubes (CNTs) and graphene. The hybrid structure containing Ag NWs-CNT [39]–[41] and Ag NWs-graphene [42]–[44] was reported in many publications. Fabrication via vacuum filtration method is generally preferred to obtain these hybrids.

Zang et al.[44] reported a Ag NWs-graphene hybrid structure that was used as a thin film heater. It was indicated that both the oxidation stability and heating performance were enhanced following the formation of Ag NWs-graphene hybrid structure. Figure 2. 8 (a) show the resistance change with time for pristine Ag NWs and Ag NWs-graphene hybrid electrodes under ambient conditions and at 100 °C. After 72 hours of measurement, sheet resistance of bare Ag NW networks electrode increased whereas Ag NWs-graphene hybrid electrode preserved its initial sheet resistance values. Figure 2. 8 (b) and (c) show the time dependent heating profile under 10 V applied voltage for pristine Ag NWs and Ag NWs-graphene hybrid (annealed at different temperatures) electrodes, respectively, and that of hybrid film under different applied potentials. It is clear that steady-state temperatures were higher for all hybrid structures than the pristine Ag NWs electrode. Moreover, steady state temperatures of 68, 150 and 230 °C were achieved under 5, 10, and 15 V applied potentials, respectively. As a result, heating performance for Ag NWs-graphene hybrid structure was found to get enhanced.

Ag NWs- single walled CNT (SWCNT) hybrid structure was studied by Shobin et al.[39] to determine their ammonia sensing performance. In the sensor, resistance of SWCNT changed to a steady state value due to a charge transfer occurred upon exposure to ammonia. Sensing response time of the device with Ag NWs-SWCNT hybrid structure was reduced 7.75 times of that of SWCNT, shown in Figure 2. 8 (d) since the charge transfer became faster. It was also found that the sensor response decreases as the amount of Ag NWs loading increases. Figure 2. 8 (e) provides the ammonia response of the SWCNT with various Ag NWs amounts.

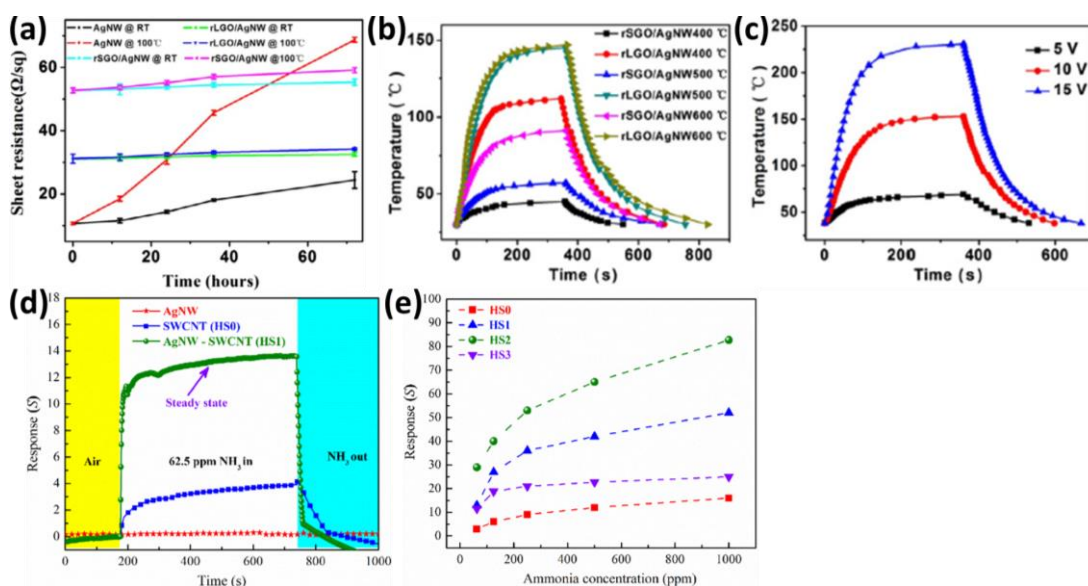


Figure 2. 8 (a) Time dependent sheet resistance change for pristine Ag NWs and Ag NWs-graphene hybrid electrodes, (b) Temperature profiles for pristine Ag NWs and Ag NWs-graphene hybrid (annealed at different temperatures) electrodes and (c) temperature profile for Ag NWs-graphene hybrid electrodes under different applied potentials [44]. (d) Ammonia responses of Ag NWs, SWCNT and Ag NWs-SWCNT sensors and (e) ammonia response of SWCNT with various Ag NWs amounts [39].

2.3. Experimental Procedure

All chemicals used in the experiments were purchased from Sigma-Aldrich and used without further purification. The chemicals were ethylene glycol (anhydrous, 99.8%), silver nitrate (ACS reagent, $\geq 99.0\%$), polyvinylpyrrolidone (PVP) (powder, average Mw $\sim 55,000$), sodium chloride (ACS reagent, $\geq 99.0\%$), acetone (ACS reagent, $\geq 99.5\%$), ethanol (absolute, $\geq 99.8\%$), nitric acid (ACS reagent, 70%), L-Ascorbic acid (ACS reagent, $\geq 99\%$), chloroplatinic acid (8 wt% in H_2O), polyvinylpyrrolidone (MW 55000) and diethylhydroxylamine ($\geq 98\%$) were supplied from Sigma-Aldrich, on the other hand, sodium hydroxide (pellets pure, $\geq 99\%$) was supplied from Merck.

All glassware and magnetic stirrers were cleaned prior to the experiments. They were first washed with Alconox detergent and rinsed with DI water. Afterwards, magnetic stirrers were cleaned through ultrasonication in 10 % nitric acid-DI water solution and then, rinsed with DI water. Finally, both the glassware and magnetic stirrers were ultrasonicated in acetone, ethanol and DI water (15 min each).

2.3.1. Synthesis of Ag NWs

Ag NWs were synthesized using an improved polyol recipe initially developed by Coskun et al.[10]. In a typical synthesis, two separate solutions were prepared. The first solution, which was named as “Solution-A” contained 80 ml EG 0.45 M PVP (MW = 55K g/mol) and 1 mM NaCl in a 100 ml beaker. After adding PVP and NaCl into EG, the suspension was stirred at 1000 rpm under 90 °C for 20 min. This dissolved all solids in the EG and the solution was cooled down to room temperature. The second solution, named as “Solution-B” contained 0.12 M AgNO₃ in 40 ml EG in a 250 ml round bottom single neck flask. It was placed in a dark box and stirred at 1000 rpm at room temperature for 20 min until all AgNO₃ dissolved. The Solution-B was placed in a preheated silicon oil bath at 120 °C with 1000 rpm stirring. Within a few minutes, dropwise addition of Solution-A into hot Solution-B was performed with the help of a disposable pipette. Dropwise addition of Solution-A took 5-7 min after which the temperature of the silicon oil bath was immediately raised to 160 °C. At the same time, distillation column of the reflux system was placed into the neck of the flask. Ag NW synthesis reaction took place at 160 °C for 80 min.

Photographs given in Figure 2. 9 (a)-(c) show the color change during the polyol synthesis of the Ag NWs from the beginning to the end of synthesis. In the early stage of the synthesis, Ag⁺ ions form and Ag NPs nucleate due to the reduction of ions to metallic Ag. During the synthesis, one dimensional growth of Ag NWs take place and color of the reaction medium starts to change. Grey-like color that appears at the end of the process indicates the formation of Ag NWs.

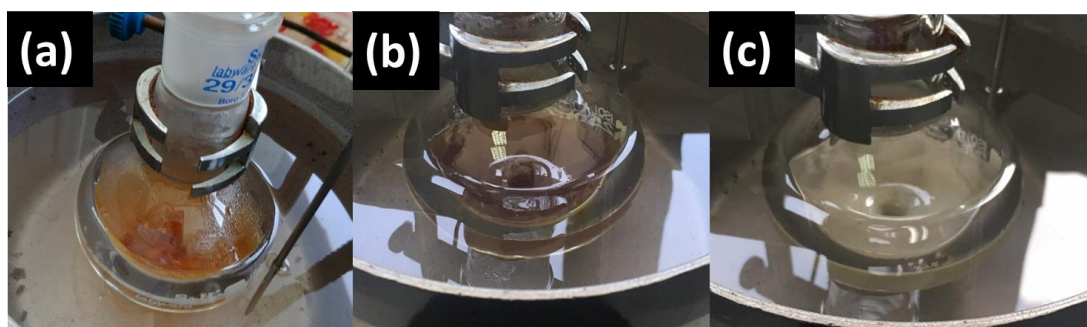


Figure 2. 9 Photographs showing the color change during the polyol synthesis of Ag NWs after (a) 1 min (b) 40 min and (c) 80 min.

Following synthesis, Ag NWs were purified to get rid of the synthesis by products, PVP, EG and Ag particles. Purification was practiced via decantation, multi-step centrifuging and sedimentation. A few days after decantation of Ag NWs, the excess suspension which contained PVP, reacted EG and Ag NPs was removed from NWs. The remaining suspension was diluted with acetone at a 1:4 ratio to dissolve any residue of PVP and EG in acetone. The suspension was centrifuged with 7000 rpm for 3 min. The supernatant mainly contained the Ag NPs and other polymeric residues. The solid that settled to the bottom of the centrifuge tube was mainly synthesized Ag NWs. The separated Ag NWs were mixed with 200 ml of ethanol and the resulting suspension was twice centrifuged with 7000 rpm for 6 min. The centrifuged ethanol suspension contained micron-size silver particles and mainly Ag NWs. To get rid of these unwanted particles, the sedimentation was applied in ethanol three or five times. Finally, a purified ethanolic Ag NWs dispersion was obtained. The ethanolic Ag NWs dispersion was used for further characterization and utilization.

2.3.2. Synthesis of Ag-Pt Core-Shell NWs

The core-shell Ag-Pt NW synthesis was originated from the work by Stewart et al. [29] where Cu NWs were decorated with Ag, Au and Pt. The constituents were Ag NWs as nucleation site, ascorbic acid (AA) as reducing agent and PVP as capping agent and chloroplatinic acid (H_2PtCl_6) as Pt source. Sodium hydroxide (NaOH) was also used in some experiments to alter the pH of the reaction medium.

Pt coating started with the preparation of 2.0 ml of 5 wt% of PVP-DI water solution and 5.5 ml of 1 M AA-DI water solution. By mixing those two solutions, 7.5 ml solution of AA and PVP was obtained and vigorously stirred at least for 3 minutes at 750 rpm until all the reagents were dissolved and a clear solution was obtained. Then, 3.0 ml of 0.5 mg/ml Ag NWs-DI water suspension was added into the AA-PVP solution under stirring. The suspension was kept mixing for a few minutes. In another beaker, aqueous chloroplatinic acid solution was prepared with a concentration of 0.01 M. After that, different amounts of 0.01 M aqueous chloroplatinic acid solution; 0.10 ml, 0.47 ml, 0.71 ml and 0.95 ml was added into the reaction medium for parametric studies. The suspension was stirred for 5 minutes at 500 rpm. Following the complete reduction of chloroplatinic acid, the suspension was centrifuged 3 times with excess DI water at 8000 rpm and once with ethanol to remove the unreacted polymers and organics. In addition to a typical synthesis route, some of the parameters were changed to investigate their effects on nucleation of Pt on Ag NWs, which are shown in Table 2. 1.

Table 2. 1 Investigated parameters and the reasoning.

Changed Parameters	Comments
Chloroplatinic Acid Solution Amount	To determine the optimum value
Without Chloroplatinic Acid Solution	To determine the effect of PVP-AA solution on Ag NWs
pH of Reaction Medium	To observe the effect of pH on final NWs
DEHA Addition	To avoid NWs shortening
Temperature	To reduce the reaction kinetic
Injection Rate of Chloroplatinic Acid Solution	To reduce Pt deposition rate

2.4. Nanowire Characterization Methods

2.4.1. Scanning Electron Microscope (SEM)

The synthesized bNWs were examined under field emission scanning electron microscope (FE-SEM) (Nova NanoSEM 430). The operation voltage was 10 kV,

15kV or 20kV. Dried Ag NWs on silicon wafers were used for SEM characterization. Silicon wafers were attached to the SEM holder using double sided carbon tape. No gold or carbon coating was applied to these samples.

2.4.2. Transmission Electron Microscope (TEM)

Further morphological analysis of the synthesized Ag NWs were conducted using transmission electron microscope (TEM) operated at 200 kV under high-resolution mode (HR-TEM)(JEOL JEM-2100F UHR/HRP 200 kV). TEM samples were simply prepared by drop casting the ethanolic Ag NWs suspension onto holey carbon coated 400 mesh copper grids.

2.4.3. X-Ray Diffraction Analysis (XRD)

XRD analysis was used to determine the crystal structure of Ag NWs. X-ray diffraction (XRD) measurements were conducted using a Rigaku D/Max-2000 diffractometer with Cu K α radiation at an operating voltage of 40 kV within 2 θ range of 20-80° at a scanning rate of 1 °/min.

2.4.4. X-Ray Photoelectron Spectroscopy (XPS)

X-Ray photoelectron spectroscopy (XPS) was performed using PHI 5000 versaprobe (XPS) spectrometer with Al-monochromatic X-rays and the operation power of ion gun was 500 eV-5 keV. XPS peak fitting was solved in OriginPro 2016 software such that every data points were fitted to Gaussian-Lorentzian function with the baseline correction to form the most suitable peaks. Carbon (1s) line was chosen as reference line at 286 eV which was set as charge correcting of binding energies.

2.4.5. pH Measurements

The scientific Orion 3-star conductivity meter was used to measure the pH values of solution during Pt coating. The measurements were done as follows; at first, pH probe was rinsed with DI water and dried with lint free laboratory napkin without rubbing the glass surface of the probe. Secondly, pH probe was dipped into the solution until

pH meter showed a steady value. Lastly, pH probe was rinsed with excess amount of DI water and kept in storage solution.

2.5. Results

2.5.1. Bare Silver Nanowires

Figure 2. 10 (a) indicates that the Ag NWs with an average diameter of 52.4 ± 3.8 nm were synthesized under the described conditions. In addition, average length of the nanowires was measured as 9.5 ± 2.4 μ m. Randomly selected nanowires were used for the diameter and length calculations. Moreover, Figure 2. 10 (a) signifies the purity of the nanowires since the SEM image is dominated with Ag NWs and almost no Ag NPs are observed.

Figure 2. 10 (b) shows a HR-TEM image of the purified Ag NWs. HR-TEM image revealed that perfect crystallinity and smooth surface of the Ag NWs. Moreover, a 3-5 nm thick PVP layer was also evident on the Ag NWs, which is useful for the dispersion of NWs.

XRD pattern of the purified Ag NWs is provided in Figure 2. 10 (d). Two peaks at diffraction angles of 33.2° and 44.8° correspond to (111) and (200) planes of the face centered cubic (FCC) Ag crystal, respectively. No other peaks were observed signifying the purity of the synthesized Ag NWs within the resolution of XRD method.

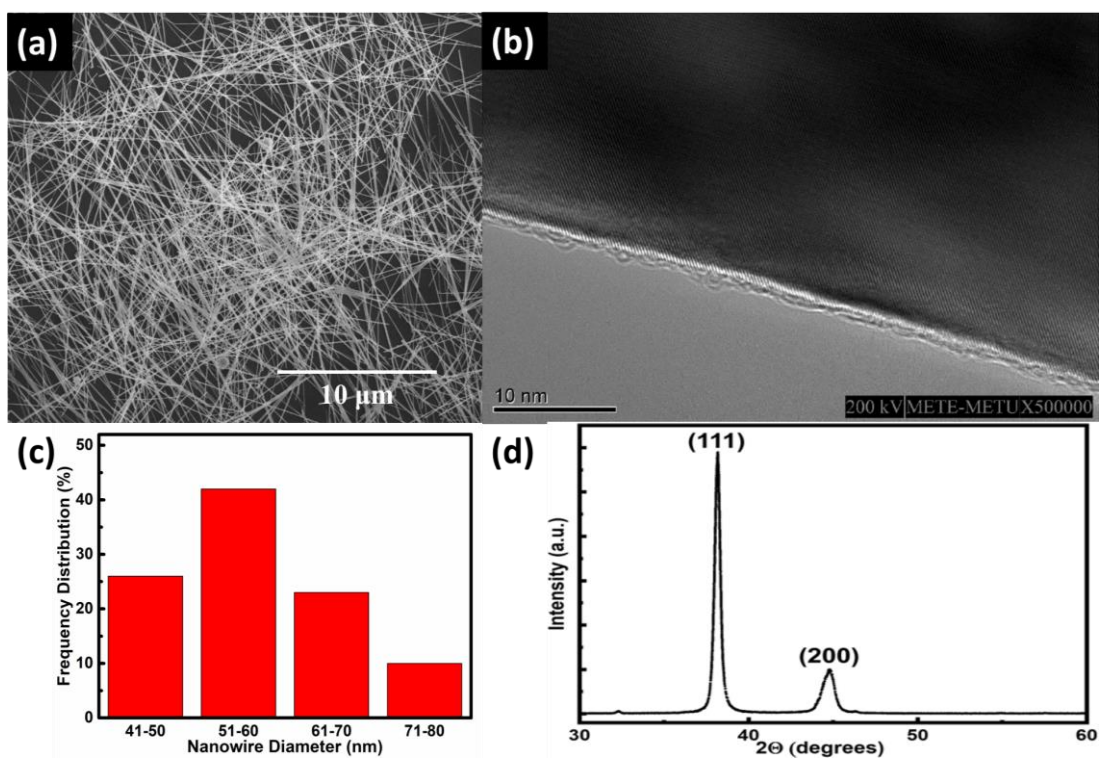


Figure 2. 10 (a) HR-TEM image (b) SEM image (c) Diameters distribution and (d) XRD pattern of purified Ag NWs synthesized via polyol method. (JCPDS Card no: 04-0483).

2.5.2. Ag-Pt Core-Shell NWs

The first core-shell NW synthesis was conducted using 5.5 ml of 1 M AA and 2.0 ml of 5 wt % PVP in DI water, into which a 0.5 mg/ml Ag NW DI water suspension was poured and a suspension having pH value of 2.3 was obtained. 0.95 ml of 0.01 M chloroplatinic acid solution was put in the reaction medium using a micro pipette. SEM and TEM images of the synthesized core-shell nanowires are given in Figure 2. 11 (a) and (b), respectively. From the SEM image, the average diameter of the Ag-Pt core-shell NWs was calculated as 96.2 ± 9.5 nm. The increase in the diameter due to Pt coating was very clear since the average diameter of bare Ag NWs was stated previously as 52.4 ± 3.8 nm. Roughly a 40 nm increase in diameter of NWs was observed. Moreover, there was no galvanic replacement between Ag and Pt since the surface of the core-shell NWs were rather smooth with no holes. TEM image clearly

showed a conformal coating of Pt over Ag NWs. TEM image also revealed the core-shell structure that was highly homogeneous and galvanic replacement free.

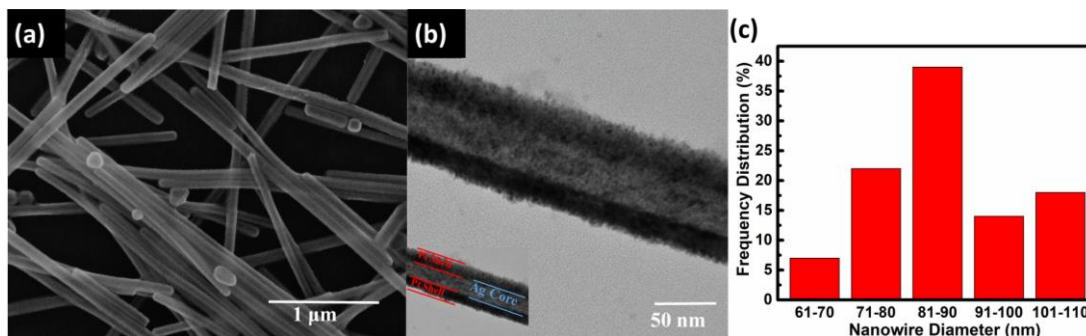


Figure 2. 11 (a) SEM and (b) TEM images and (c) diameter distribution of Ag-Pt core-shell NW networks using 0.95 ml of 0.01 M chloroplatinic acid solution.

Both areal and line EDS maps of the Ag-Pt core-shell nanowires on individual NW basis obtained with TEM to get a better understanding on the coating homogeneity. Figure 2. 12 shows TEM images with areal and line EDS mapping for the Ag-Pt core-shell NWs. Areal mapping of an individual nanowire is shown in Figure 2. 12 (a), (b) and (c). the shell layer and core of the nanowire were very clear due to the color contrast between Ag and Pt. This contrast, dark for Pt and light for Ag, was appeared due to the different atomic numbers of elements. In addition to color contrast, in areal mapping, both Ag and Pt atoms exist throughout the examined nanowire. Moreover, the line mapping results are shown in Figure 2. 12 (d) and (e) and it was easily deduced that relative amounts of both Ag and Pt fluctuates through the nanowire. This was because the relative amount of Pt at the edges was higher than that in the middle of NWs due to the shape of NWs. In addition to mapping, it was found that the relative amounts of Ag and Pt were 63 at.% and 37 at.%, respectively.

EDS mapping for Ag-Pt core-shell NWs was also practiced with SEM to examine in the case over larger areas. Figure 2. 13 (a) - (c) show SEM image of Ag-Pt core-shell NWs, EDS mapping for Ag and EDS mapping for Pt, respectively. This results means that there were no galvanic replacement and both Ag and Pt atoms were distributed homogeneously through the nanowires.

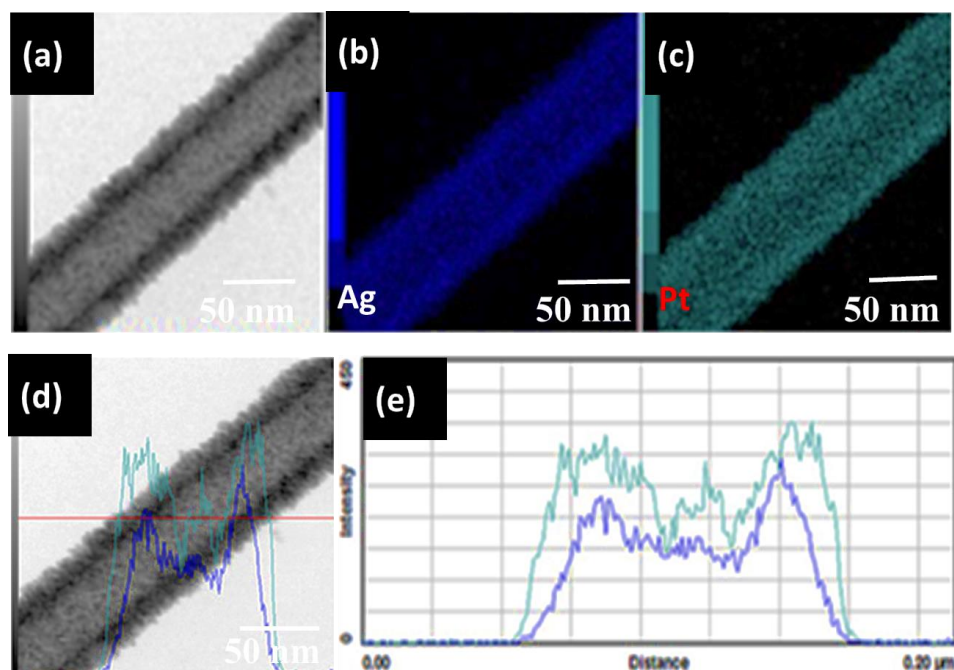


Figure 2. 12 (a) TEM image of Ag-Pt core-shell NWs, EDS mapping for (b) Ag, (c) Pt (d) EDS line mapping for Ag and Pt and (e) line profile for red line in part (d). (dark blue lines for Ag and light blue lines for Pt).

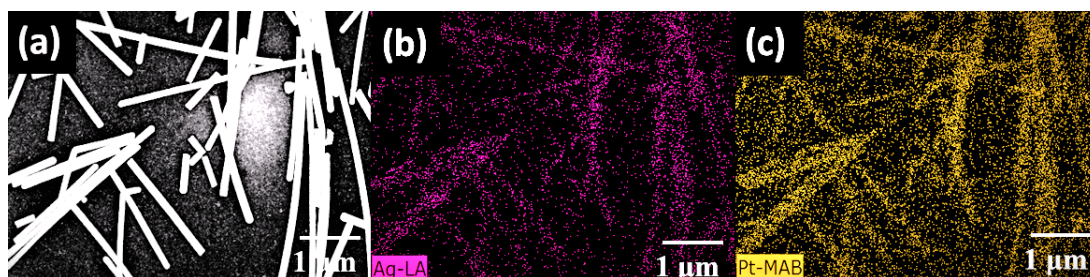


Figure 2. 13 (a) SEM image of Ag-Pt core-shell NWs, EDS mapping for (b) Ag and (c) Pt.

After ensuring that the synthesis process was successful for uniform and galvanic replacement free coating of the shell layer, experimental studies were further expanded to explore the role of chloroplatinic acid and to determine the optimum amounts of other reagents.

It is important to increase the aspect ratio (length/diameter) of the Ag-Pt core-shell NWs and to reduce the use of Pt salt. The shell layer thickness was found approximately as 22 nm. Therefore, it was crucial to lower the shell layer thickness since that would simultaneously increase the aspect ratio of the NWs and decrease the chloroplatinic acid use. By keeping the other parameters constant, the chloroplatinic

acid amount was reduced to 0.71 ml, 0.47 ml and 0.10 ml while the concentration was kept constant at 0.01 M. Figure 2. 14 shows a SEM image of the Ag-Pt core-shell NWs synthesized with 0.71 ml of 0.01 M chloroplatinic acid. As can be seen from the figure, Ag-Pt core-shell NWs had smooth surfaces no sign of galvanic replacement was found and the average diameter of NWs was measured as 87.8 ± 13.3 nm. The Pt thickness was still considered to be high for transparent conducting thin film applications.

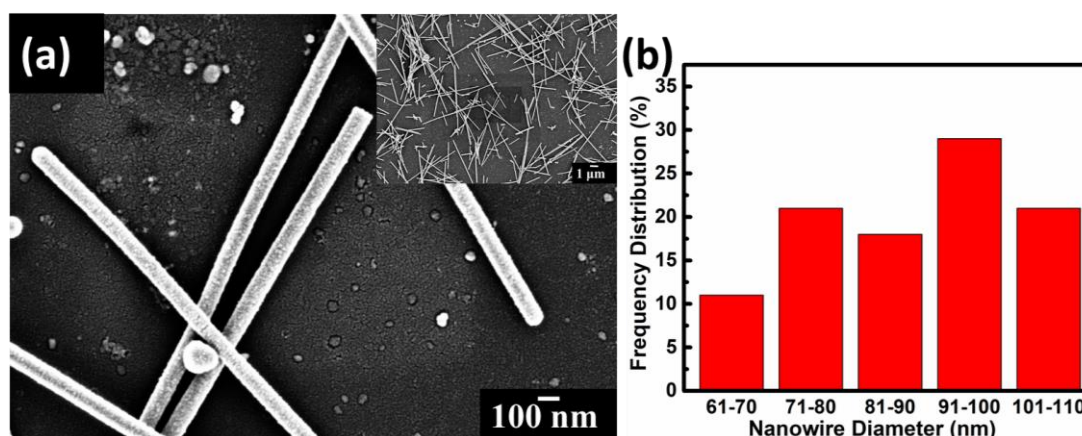


Figure 2. 14 (a) SEM image (inset shows a low magnification SEM image) and (b) diameter distribution of Ag-Pt core-shell NWs synthesized using 0.71 ml of 0.01 M chloroplatinic acid.

SEM image of Ag-Pt core-shell NWs synthesized using 0.71 ml of 0.01 M chloroplatinic acid and the corresponding EDS maps for Ag and Pt are shown in Figure 2. 15 (a) – (c), respectively. Results were found to be similar to those obtained for 0.95 ml of 0.01 M chloroplatinic acid use and no galvanic replacement was observed. Pt atoms were uniformly distributed throughout the NWs.

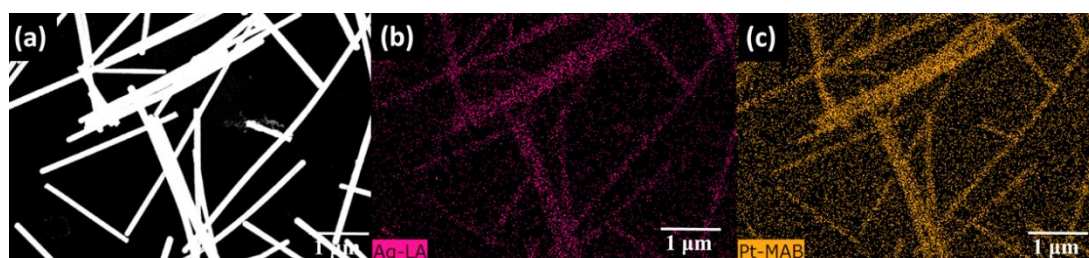


Figure 2. 15 (a) SEM image of Ag-Pt core-shell NWs synthesized using 0.71 ml of 0.01 M chloroplatinic acid. EDS maps for (b) Ag and (c) Pt.

In the following synthesis, 0.47 ml of 0.01 M chloroplatinic acid was used to reduce the Pt salt use and the shell thickness. Figure 2. 16 shows SEM image of the Ag-Pt core-shell NWs synthesized using 0.47 ml of 0.01 M chloroplatinic acid. Galvanic replacement free and homogeneous Ag-Pt core-shell NWs were successfully synthesized. The average diameter of Ag-Pt core-shell NWs synthesized using 0.47 ml of 0.01 M chloroplatinic acid was 81.8 ± 13.6 nm. In addition, EDS analysis was also performed in SEM and relative atomic percentages of Ag and Pt atoms were obtained as 75 and 25 at.%, relatively (63 and 37 wt.%), which indicated the presence of Pt atoms on Ag NWs.

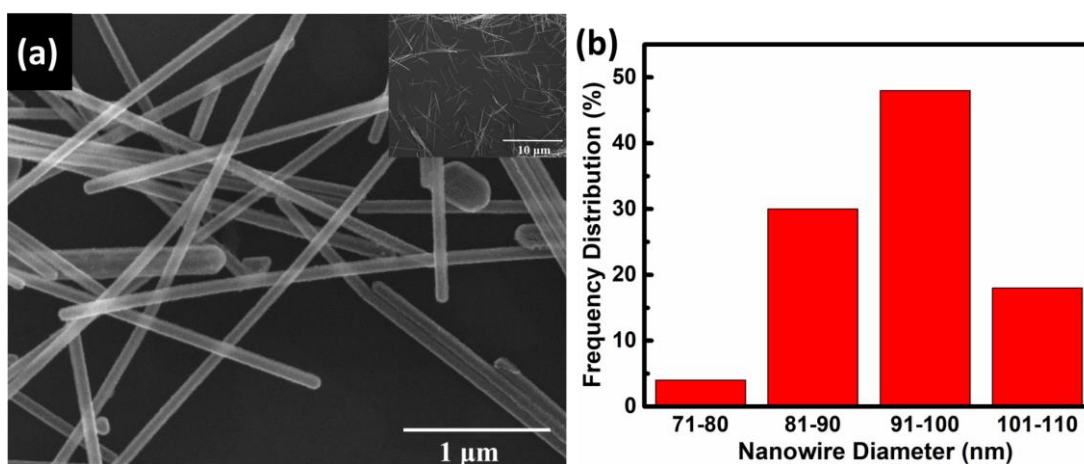


Figure 2. 16 (a) SEM image (inset shows low magnification SEM image) and (b) diameter distribution of Ag-Pt core-shell NWs with 0.47ml of 0.01 M chloroplatinic acid.

TEM image of an individual Ag-Pt core-shell NW synthesized using 0.47 ml of 0.01 M chloroplatinic acid is shown in Figure 2. 17 (a). TEM image shows a very homogeneous and conformal coating. Figure 2. 17 (b) and (c) shows the EDS area mapping results for Ag and Pt, respectively. Ag is self-explanatory; but, Pt mapping showed homogeneous distribution of Pt along the NW. The line mapping and distribution pattern, in Figure 2. 17 (d) and (e), were also supported the results that obtained with other characterization methods.

Figure 2. 17 (g) - (h) show SEM images of Ag-Pt core-shell NWs synthesized using 0.47 ml of 0.01 M chloroplatinic acid and corresponding areal maps for Ag and Pt.

EDS mapping results proved that synthesized NWs were galvanic replacement free and Pt shell layer encapsulated them. Moreover, EDS maps for an individual Ag-Pt core-shell NW synthesized using 0.47 ml of 0.01 M chloroplatinic acid were promoted by larger area EDS maps performed in SEM.

XPS results of Ag-Pt core-shell NWs synthesized using 0.47 ml of 0.01 M chloroplatinic acid are provided in Figure 2. 17 (i) and (j) for Ag and Pt, respectively. XPS deconvoluted spectra of Ag (3d) and Pt (4f) was provided showing the curve fits and peak positions. The peak positions are registered as 365.1 and 371.1 eV for Ag ($3d_{5/2}$) and Ag ($3d_{3/2}$), respectively. The positions of the 3d orbitals for metallic Ag were at 368.3 eV and 374.3 eV. Therefore, the shift in the peak position was explained in such a way that Ag atoms in core-shell NWs was interacted with its environment and lowered its binding energies [45]. On the other hand, peak positions of Pt (4f) appeared at 68.3 and 71.5 eV for Pt ($4f_{7/2}$) and Pt ($4f_{5/2}$), respectively. Binding energies of Pt ($4f_{7/2}$) and Pt ($4f_{5/2}$) for bulk Pt are 72 and 75 eV, respectively. The shift of peak position was associated with the encapsulation of outer Pt shell layer with PVP [46]. Lastly, XPS results were indicated that both Ag and Pt were in metallic form.

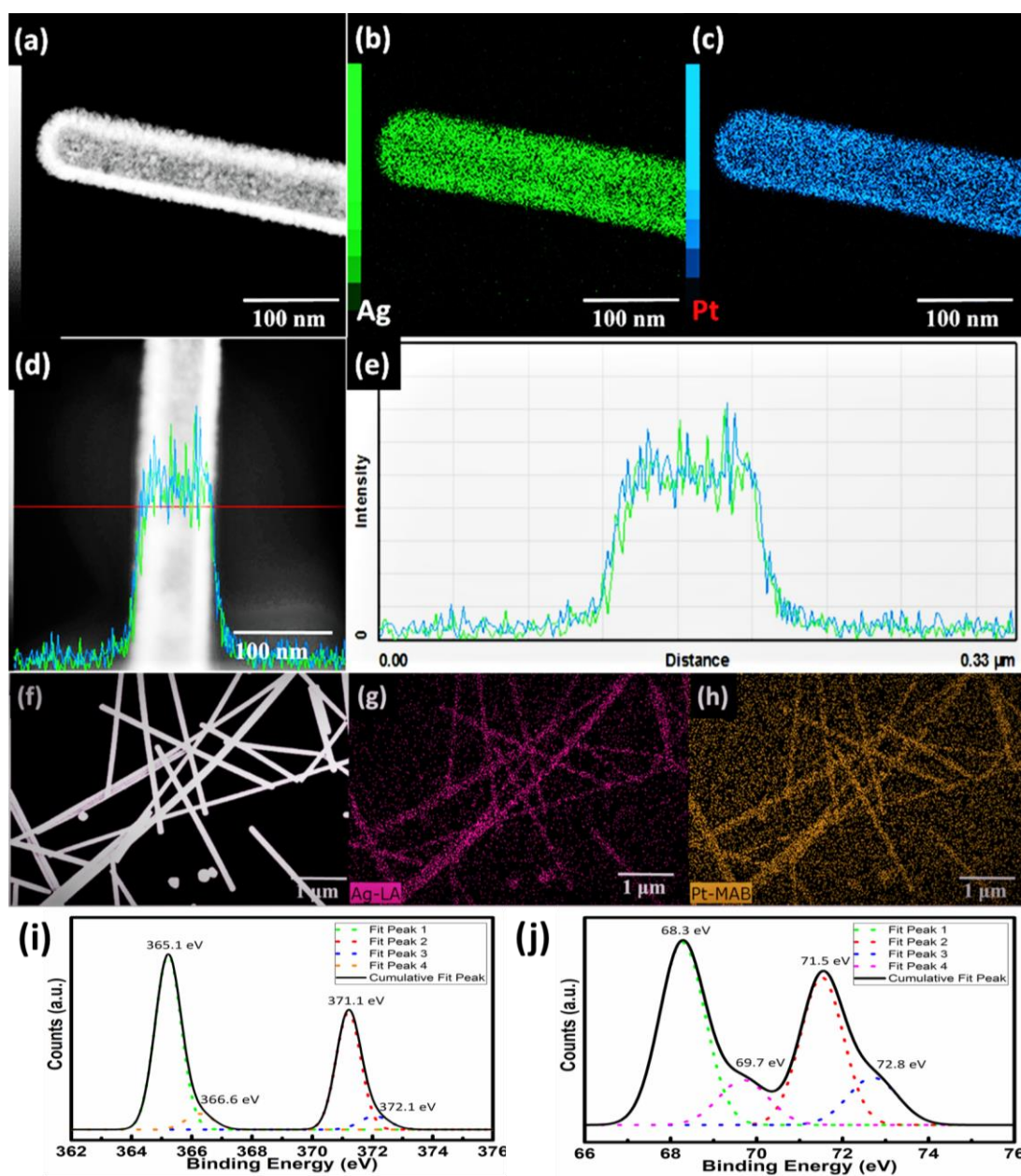


Figure 2. 17 (a) TEM image of Ag-Pt core-shell NWs synthesized using 0.47 ml of 0.01 M chloroplatinic acid. EDS map for (b) Ag and (c) Pt, (d) EDS line map for Ag and Pt and (e) Line profile for red line in part (d). (dark green lines for Ag and light blue lines for Pt in part (b), (c), (d) and (e)) (f) SEM image of Ag-Pt core-shell NWs. EDS maps for (g) Ag and (h) Pt. XPS curve fitting for (i) Ag and (j) Pt.

Although the Ag-Pt core-shell NW synthesis using 0.47 ml 0.01 M chloroplatinic acid was adequate for reducing the amount of Pt salt use and galvanic replacement free deposition, reduction of Pt salt amount was applied one more time. In this regard, Ag-Pt core-shell NWs with 0.10 ml of 0.01 M chloroplatinic acid was synthesized keeping

other parameters the same as previous synthesis routes. Figure 2. 18 shows a SEM image of Ag-Pt core-shell NWs with 0.10 ml of 0.01 M chloroplatinic acid. From the SEM images, the average diameter of the Ag-Pt core-shell NWs was calculated as 63.1 ± 7.1 nm and the relative atomic percentages of Ag and Pt were obtained as 89 and 11 at.%, respectively (81 and 19 wt.%). Although the coating with 0.10 ml of 0.01 M chloroplatinic acid seemed to be successful in terms of galvanic free coating and presence of Pt on Ag, in Figure 2. 18 (a), EDS maps in SEM revealed that Pt coating was not sufficient and Pt particles on Ag NWs were formed. Pt particles appeared as small islands on nanowire surfaces as shown in Figure 2. 18 (b). Moreover, EDS maps for Ag and Pt are provided in Figure 2. 18 (c) and (d), respectively. Maps revealed insufficient Pt coating such that expected Pt atoms did not appear on top-right side of Figure 2. 18 (d), where Ag atoms were present as shown in Figure 2. 18 (c).

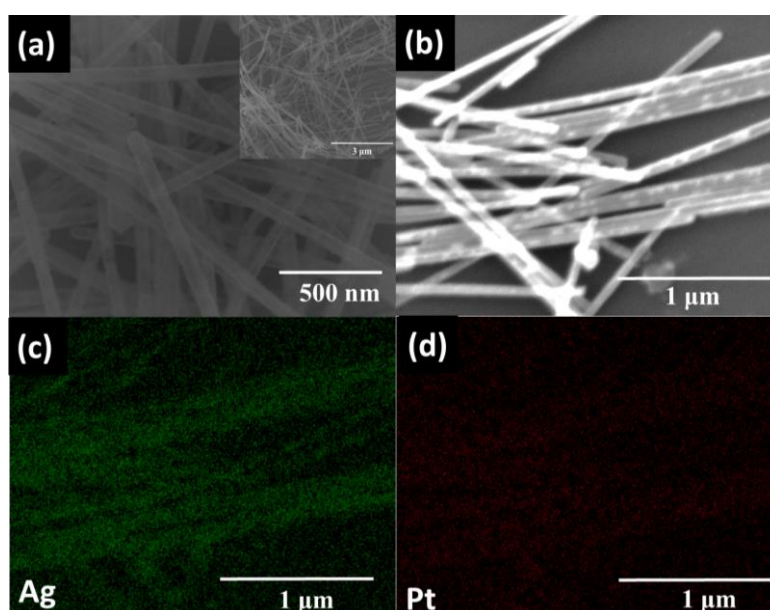


Figure 2. 18 (a) SEM images of Ag-Pt Core-Shell NWs synthesized using 0.1 ml of 0.01 M chloroplatinic acid. (inset shows low magnification SEM image). (b) SEM image used for EDS areal mapping. EDS maps for (c) Ag and (d) Pt.

As a result, considering SEM, TEM, and XPS results, optimum chloroplatinic acid amount for the synthesis of Ag-Pt core-shell NWs was determined to be 0.47 ml. Average diameter of the Ag-Pt core-shell NWs and relative atomic percentage of Ag and Pt are provided in Table 2. 2. As the objective was to reduce the use of

chloroplatinic acid solution while having a relatively thick shell layer, Ag-Pt core-shell NWs synthesized using 0.47 ml of 0.01 M chloroplatinic acid were used in applications with enhanced nanowire stability. The only disadvantage associated with this synthesis was the reduction in the length of the nanowires compared to their as-synthesized counterparts.

Table 2. 2 Average diameter and relative atomic percentage for Ag and Pt obtained from synthesis using different chloroplatinic acid amount.

Chloroplatinic Acid Amount (ml)	Average Diameter (nm)	Relative Atomic Percentage Ag (at%)	Relative Atomic Percentage Pt (at%)
0.95	96.2 ± 9.5	63	37
0.71	87.8 ± 13.3	66	34
0.47	81.8 ± 13.6	75	25
0.10	63.1 ± 7.1	89	11

However, other than chloroplatinic acid solution concentration, effects of synthesis conditions on the morphology of the NWs were also examined. To observe the effect of AA and PVP on Ag NWs, the synthesis started with treatment of Ag NWs with AA-PVP solution without chloroplatinic acid solution. The synthesis was conducted in such way that 2.0 ml of 1 M AA and 5.5 ml of 5 wt% PVP solutions were stirred at 750 rpm using a magnetic stirrer. Afterwards, 3.0 ml of 0.5 mg/ml Ag NWs-DI water suspension was poured into the solution and mixed for another 5 minutes. At the end, same centrifuge steps, as aforementioned before, were used to purify the NWs. SEM image of Ag NWs, that were treated with AA-PVP solution, is shown in Figure 2. 19. Sharp bending and breaking of NWs were observed and encircled by red circles in the figure. The average length of NWs was calculated as $4.9 \pm 2.4 \mu\text{m}$ which was smaller than that of bare Ag NWs. This signifies, shortening of NWs was occurred while Ag NWs were exposed to AA-PVP solution.

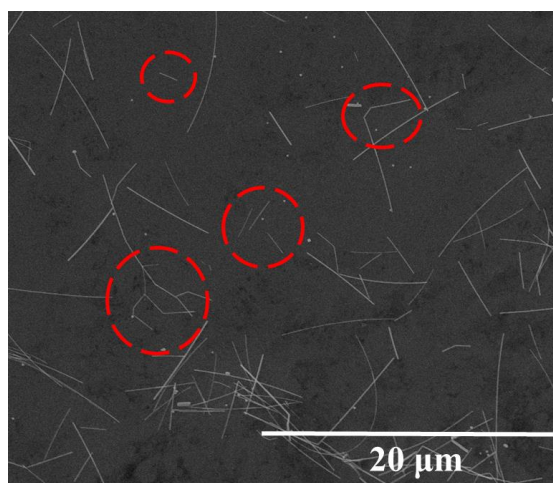


Figure 2. 19 SEM image of Ag NWs exposed to AA-PVP solution.

Therefore, shortening problem of Ag NWs was tried to be avoided in the further synthesis attempts. Ag-Pt core-shell NW synthesis was started to be controlled by a pH meter. To observe the effect of reaction pH on the synthesis and most importantly to prevent the decrease in length of NWs, synthesis reactions were designed with different pH values. The attempts with controlled pH values were done according to the basis of the Ag-Pt core-shell NWs synthesis using 0.47 ml chloroplatinic acid solution.

Initial synthesis suspension which involved AA, PVP and Ag NWs in DI water was prepared and the pH value was measured as 2.3, which meant that the coating was performed in an acidic medium. In order to synthesize core-shell NWs within a basic medium, 1 M of aqueous NaOH solution was added dropwise to the initial suspension until a pH value of 8.0 was reached. Later, 0.47 ml of 0.01 M chloroplatinic acid solution was added to this suspension having a pH value of 8.0. Following the addition of Pt salt, while the solution was stirred at 500 rpm via a magnetic stirrer, the solution pH dropped to 6.3. After a few minutes, the resulting solution was centrifuged multiple times to remove the residues. The synthesized Ag-Pt core-shell NWs was examined using SEM, an image of which is provided in Figure 2. 20. The average NW diameter was calculated as 67.2 ± 7.9 nm and the relative atomic percentages of Ag and Pt which were obtained via EDS data were 95 and 5 at.%, respectively. Particles were

observed to nucleate on the surface of Ag NWs rather than spreading homogeneously along the NW surface. Moreover, the length of the synthesized Ag-Pt core-shell NWs was observed that there was no deviation from the synthesis performed in basic medium.

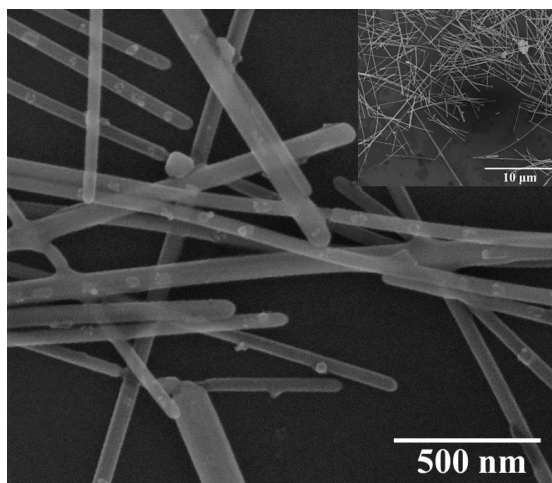


Figure 2. 20 SEM image of Ag-Pt core-shell NWs synthesized in a reaction medium with a pH value of 8.0 (inset shows low magnification SEM image).

Other pH controlled Ag-Pt core-shell NWs synthesis was conducted in acidic medium where the pH value of the reaction medium was set to 4.0. The reaction medium was selected to be acidic since the conformal Pt coating on Ag did not be achieved in basic medium (pH 8.0). AA, PVP and Ag NWs suspension was prepared and 1 M of NaOH was added dropwise into the solution until the pH value of the suspension reached 4.0. A SEM image of the Ag-Pt core-shell NWs synthesized in reaction medium with a pH value of 4.0 is shown in Figure 2. 21. The average diameter and length of Ag-Pt core-shell NWs were calculated as 72.7 ± 7.3 nm and 4.6 ± 1.5 μ m. Therefore, it is evident that the drop in the average length of synthesized Ag-Pt core-shell NWs could not be prevented using this method. Moreover, the surface roughness of the Ag-Pt core-shell NWs was increased found to increase compared to those NWs synthesized at a pH value of 8.0.

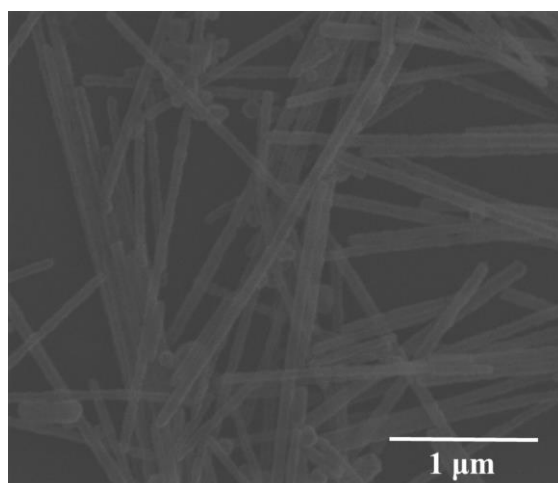


Figure 2. 21 SEM image of Ag-Pt core-shell NWs synthesized in a reaction medium with a pH value of 4.0.

As stated before, Pt coating was inspired from the work of Stewart et al. [29] where a Cu NW suspension was stored in 1 wt % PVP and 3 wt % DEHA. Thus, the storage suspension containing Cu NWs, PVP and DEHA was used for core-shell NWs synthesis. A similar storage suspension was prepared for the synthesis of Ag-Pt core-shell NWs. 305 μL of DEHA was first mixed with 3.0 ml 0.5 mg/ml Ag NWs-DI water suspension and AA and PVP solution was prepared as previously described. Afterwards, freshly prepared Ag NWs-DI water suspension with DEHA was poured into the solution. Following the chloroplatinic acid solution addition, the Ag-Pt core-shell NWs were separated from the byproducts by multiple centrifugation cycles. SEM image of synthesized Ag-Pt core-shell NWs is shown in Figure 2. 22 and the average diameter and length of the NWs were determined as 62.2 ± 6.3 nm and 9.5 ± 3.6 μm , respectively. As a result, the shortening of the NW was avoided. However, this time, diameters of the NWs were increased inadequately for the thin film applications.

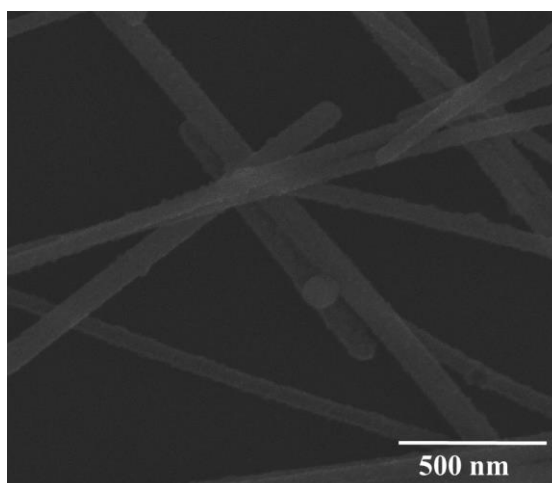


Figure 2. 22 SEM image of Ag-Pt core-shell NWs where DEHA-Ag NWs suspension was used.

Next, the synthesis in an ice bath was conducted to reduce the reaction rate between the solution containing AA, PVP and Ag NWs and to maintain NW integrity after Ag NWs were added into the AA-PVP solution. For the mentioned purpose, the whole process of Ag-Pt core-shell NWs synthesis was conducted in an ice bath and the temperature of the bath was measured with a mercury thermometer and kept at 5 °C throughout the synthesis. First, a 25 ml beaker was placed into an ice bath, then 2.0 ml of 5 wt% of PVP and 5.5 ml of 1 M AA DI water solutions were mixed at 750 rpm. After the solution became clear, first 3.0 ml of 0.5 mg/ml Ag NWs-DI water suspension was added which is followed by addition of 0.47 ml of 0.1 M chloroplatinic acid. The suspension was stirred for 15 minutes at 500 rpm in the ice bath. At the end, multistep centrifugation was performed for purification using cold DI water and ethanol. Figure 2. 23 shows a SEM image of the Ag-Pt core-shell NWs synthesized in the ice bath. The average NW length was calculated as $6.7 \pm 1.0 \mu\text{m}$ and EDS results revealed the atomic percentage of Ag and Pt were 91 and 9 at.%, respectively. Therefore, Ag-Pt core-shell NWs synthesized in an ice bath had insufficient Pt coating and the reduction in NW length was still prominent.

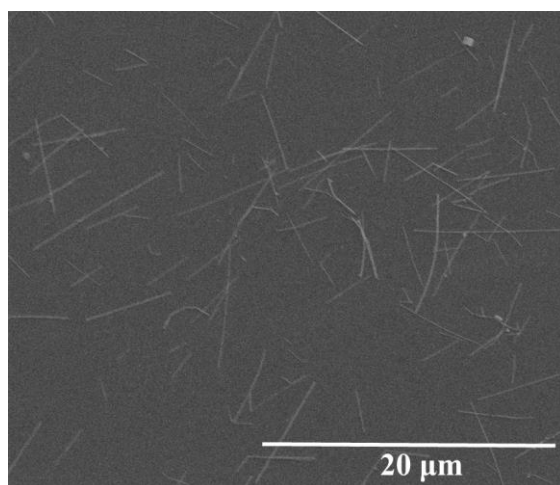


Figure 2. 23 SEM image of Ag-Pt core-shell NWs synthesized in an ice bath.

Until this point, addition of chloroplatinic acid solution into the AA, PVP and Ag NWs suspension was practiced to with a micropipette and with no control on the injection rate. A syringe pump was then used to control the injection rate of chloroplatinic acid solution and the 3 different concentrations for the injected chloroplatinic acid solution was investigated, which were 0.48 mM, 3.93 mM and 9.53 mM. Syntheses were carried on dissolution of 2.0 ml of 5 wt.% PVP and 5.5 ml of 1 M of AA solutions in DI water and addition of 3.0 ml of 0.5 mg/ml of Ag NWs-DI water suspension into the mixed solution. Then, the pH of the suspension was set to 7.2-7.5 by adding 1 M of aqueous NaOH solution to carry the experiments in a basic medium. Injection rate of the chloroplatinic acid solution was selected to be 2.7 ml/h and 10 ml of chloroplatinic acid solution was injected for each case. Figure 2. 24 (a) shows a SEM image of the Ag-Pt core-shell NWs with injection of 0.476 mM chloroplatinic acid solution and the average diameter of NWs was calculated as 56.8 ± 7.8 nm, which was close to that of bare Ag NWs. Moreover, EDS results showed that the atomic percentages of Ag and Pt were 94 and 6 at.%, respectively. These percentages were considered insufficient. Moreover, Pt particles were observed to nucleate on Nw surfaces and thus a conformal Pt coating on Ag NWs could not be obtained. Next, the concentration of chloroplatinic acid solution was first increased to 3.93 mM and then to 9.53 mM. SEM images of Ag-Pt core-shell NWs s with injection of 3.93 mM and

9.53 mM chloroplatinic acid solutions are provided in Figure 2. 24 (b) and (c), respectively. Although the concentration of injected chloroplatinic acid solution was enhanced, the SEM images obtained from these two cases did not differ from that of synthesis with a chloroplatinic acid solution of 0.47 ml of 0.01 M.

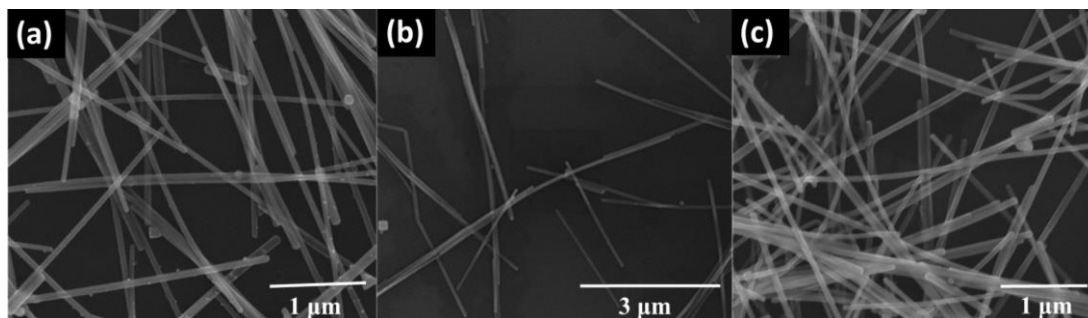


Figure 2. 24 SEM images of Ag-Pt core-shell NWs s with injection of (a) 0.48 mM, (b) 3.93 mM and (c) 9.53 mM chloroplatinic acid solution.

CHAPTER 3

SILVER PLATINUM CORE SHELL NANOWIRE NETWORKS WITH ENHANCED STABILITY

3.1. Stability of NW Networks

The drawback of Ag NW network is that they have low stabilities when integrated into an application. The low stability of the network cause both to lost the performance of in working condition and to limit the usage area. The stability of Ag NWs network is classified under electrochemical, environmental, chemical, thermal and mechanical.

3.1.1. Electrochemical Stability

Electrochemical stability of Ag NW network considered as the potential window the network without irreversible oxidation. When oxidation occurs, the resistance of networks increases gradually and becomes nonconductive. The potential window where Ag NW network experiences no oxidation is very narrow and there are studies that provide a route where it broadens.

Lee et al. [27] reported on the fabrication of Ag-Au core-shell NWs and compared electrochemical performance of bare Ag NWs and Ag-Au core-shell NW electrodes. Electrochemical measurements were conducted using a 3-electrode configuration using Ag/AgCl reference electrode and Pt wire as counter electrode. Figure 3. 1 (a) schematically shows the measurement setup. Figure 3. 1 (b) and (c) show the CV results of bare Ag NW and Ag-Au core-shell NW electrodes, respectively. It was observed that bare Ag NW electrode lost its electrical conductivity because of the low oxidation potential of Ag and irreversible oxidation that takes place at 0.5 V [47]. As a result, Ag NW network experienced a break down. On the other hand, Ag-Au core-shell NW networks withstand the oxidation for fifty cycles although the conductivity of electrode decreased due to the loss of Ag atoms from NWs. Moreover, the

capacitance of the electrode was measured as $210 \mu\text{F}/\text{cm}^2$ during charge-discharge measurements.

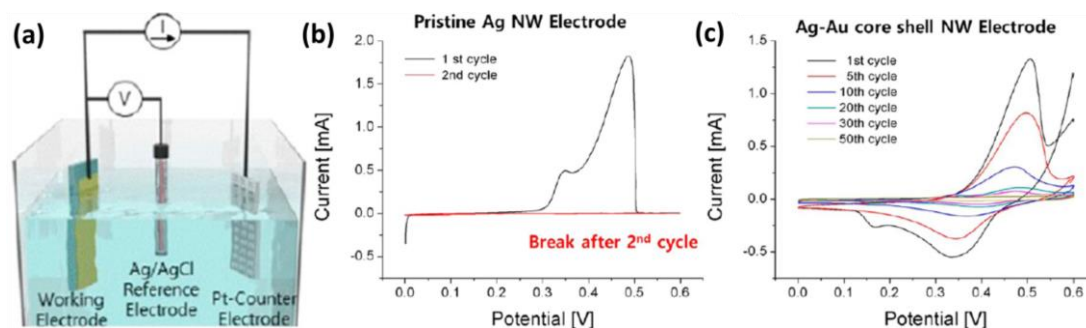


Figure 3. 1 (a) Schematic of measurement setup, (b) CV results of bare Ag NW electrode and (c) CV results of Ag-Au core-shell NW electrode [27].

Moon et al. fabricated a supercapacitor with Ag-Au-Polypyrrole (PPy) core-shell NW electrodes [48]. The electrochemical measurements were conducted in two electrode configuration using polyvinilalcohol-phosphoric acid (PVA- H_3PO_4) gel electrolyte. Figure 3. 2 (a) shows the CV results of Ag-Au-PPy core-shell NWs with different scan rates from $50 \text{ mV}/\text{s}$ to $1000 \text{ mV}/\text{s}$. At low scan rates an almost rectangular behavior was obtained, which is typical for supercapacitors. CV results of Ag-Au-PPy core-shell NWs with different PPy thicknesses are shown in Figure 3. 2 (b). It was obvious that the capacitance of supercapacitors increased with PPy thickness and the supercapacitors served within the potential range of $0\text{-}0.8 \text{ V}$. Lastly, supercapacitors with different PPy thicknesses were subject to galvanostatic charge-discharge (GCD) measurements. Figure 3. 2 (c) shows the GCD characteristics of Ag-Au-PPy core-shell NWs with different PPy thicknesses. The capacitance of the supercapacitor was found as $580 \mu\text{F}/\text{cm}^2$ for 3-cycle PPy coated Ag-Au core-shell NWs.

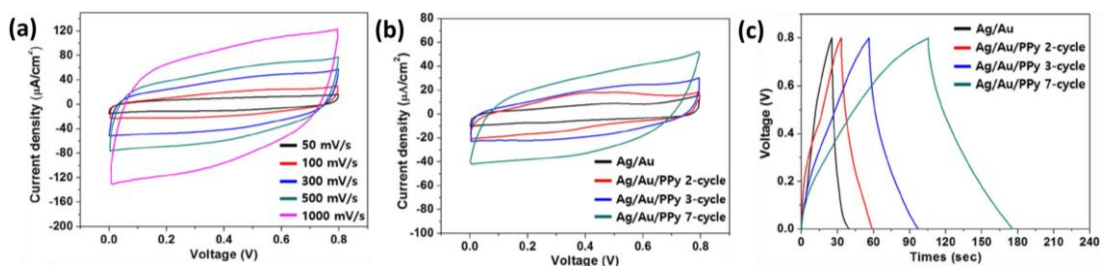


Figure 3. 2 CV results of Ag-Au-PPy core-shell NWs (a) at different scan rates, (b)) different PPy thickness.(c) Galvanostatic charge discharge results for Ag-Au-PPy core-shell NWs with different PPy thicknesses [48].

Yüksel et al. [30],[49] fabricated molybdenum (IV) oxide (MoO_2) and nickel hydroxide $\text{Ni}(\text{OH})_2$ decorated Ag NWs. Figure 3. 3 (a) and (b) shows the CV results of Ag- $\text{Ni}(\text{OH})_2$ core-shell NWs with different coating thicknesses of $\text{Ni}(\text{OH})_2$ coating thickness and at different scan rates from 2 to 100 mV/s, respectively. The specific capacitance for MoO_2 -Ag NW core-shell electrodes was determined as 500.7 F/g at a current density of 0.25 A/g. On the other hand, that of $\text{Ni}(\text{OH})_2$ -Ag core-shell NWs was measured as 1162.2 F/g at a current density of 3 A/g.

Both MoO_2 and $\text{Ni}(\text{OH})_2$ showed pseudocapacitive behaviors. As Ag NW network provided high electrical conductivity, the easiness of the charge transfer was achieved, which increased the stored energy. However, Ag NW networks could only operate in a limited potential window of 0-0.5 V [30], [49].

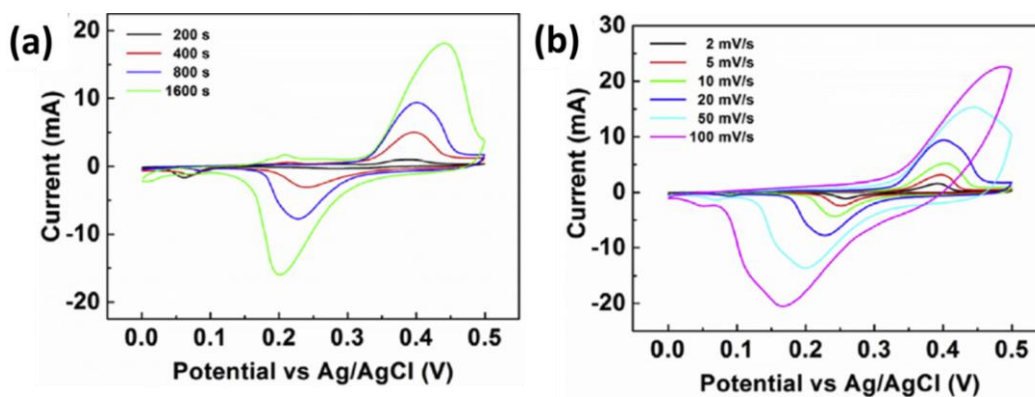


Figure 3. 3 (a) CV results of $\text{Ni}(\text{OH})_2$ -Ag core-shell NWs at different coating times and (b) different scan rates [49].

3.1.2. Environmental Stability

Environmental stability of NW networks is monitored in different relative humidity and temperature levels to create an aggressive medium.

Jui et al. [50] reported the resistance change of Ag NW networks under 85 %RH at 85 °C over 40 days. Resistance change with time was monitored for the bare Ag NW networks and that of coated with polyvinyl alcohol(PVA) and epoxy as shown in Figure 3. 4. The resistance of the Ag NW networks (triangle, square and circle in the figure) started to increase just after they placed in the relative humidity chamber. Ag NW networks coated with PVA and epoxy cannot withstand the corrosion although the degradation rate decreased.

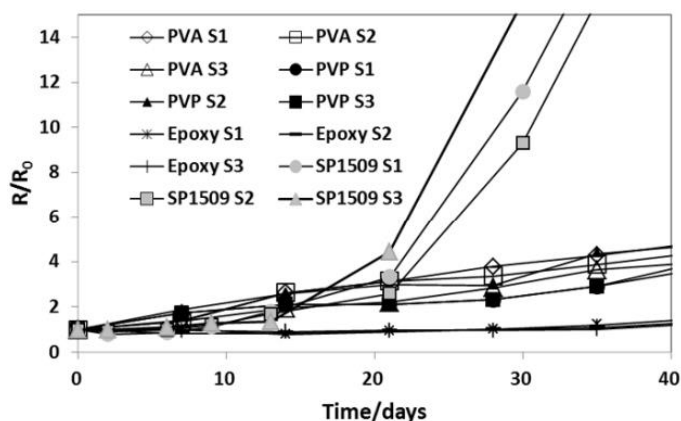


Figure 3. 4 Resistance change with time nder 85 %RH at 85 °C

3.1.3. Chemical Stability

Metals are generally prone to corrode when they are exposed to acids or bases. When Ag NW networks are exposed to either them, they are etched rapidly. In the literature, different chemicals like hydrogen peroxide (H₂O₂), sodium hydroxide (NaOH), nitric acid (HNO₃), acetic acid (CH₃COOH) are used to cause degradation Ag NW networks. The resistance change of the Ag NW networks with exposure of H₂O₂ are monitored to determine the chemical stability.

One of the study showing the resistance under the exposure of H_2O_2 was done by Lee et al. [27]. Resistance of bare Ag NWs and Ag-Au core-shell NWs networks were compared to each other, where 12.5 % H_2O_2 aqueous solution was used. Results as shown in Figure 3. 5 (a) revealed that Ag NW network degraded within seconds. On the other hand, Ag-Au core-shell NWs experienced only slight increase in resistance which contributed the dissolution of Ag from the pores of Au shell.

Choi et al. [51] studied the oxidation of Ag NWs and enhanced chemical stability of Ag-Au core-shell NWs. Both NWs were exposed to 1.5 M H_2O_2 solution for 3 hours at room temperature. TEM images for both NWs, which are shown in Figure 3. 5 (b), revealed that Ag NWs were harshly oxidized whereas Au shell protected NW from corrosion. Ultraviolet–visible spectroscopy (UV-Vis) results for Ag NWs and Ag-Au core-shell NWs are shown in Figure 3. 5 (c). After the exposure H_2O_2 solution, extinction spectrum decreases for Ag NWs but that of Ag-Au core-shell NWs remained unchanged.

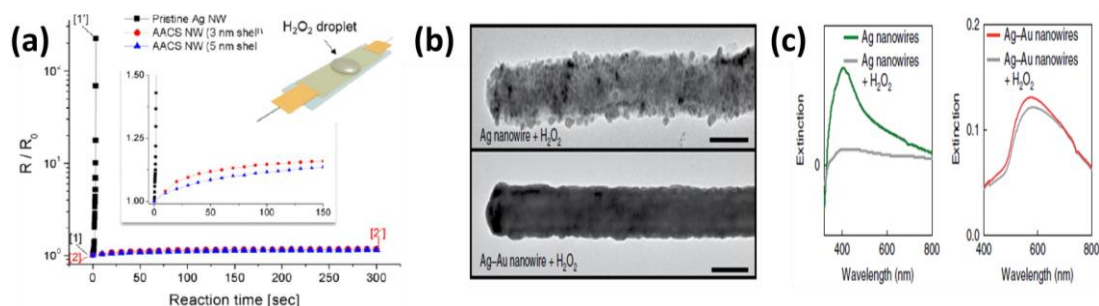


Figure 3. 5 (a) Resistance change with exposure of H_2O_2 solution time [27], (b) TEM images of Ag NW and Ag-Au core-shell NWs after exposure H_2O_2 solution (Scales are 1 μm) and (c) UV-Vis spectra of Ag NWs and Ag-Au core-shell NWs before/after exposure H_2O_2 solution [51].

3.1.4. Thermal Stability

The normal melting temperature of Ag is 962 $^{\circ}C$ [52]. The degradation of the Ag NWs occurs at much lower temperatures due to the Rayleigh instability (discussed in Chapter 4). The melting of NW take place according to the morphology of NW.

Liu et al. [53] studied the thermal stability of the Ag NWs having average diameters of 17, 45 and 120 nm. In the work, Ag NWs were also coated with 2-

mercaptobenzimidazole and octadecanethiol to compare the thermal stability with that of bare Ag NWs. Figure 3. 6 (a) shows the schematic of Ag NW and decorated Ag NWs at 300 for 50 min annealing. The melting of NW observed for bare Ag NW and octadecanethiol coated Ag NW but it was increased with mercaptobenzimidazol. The resistance change with temperature for 3 different average diameters shown in Figure 3. 6 (b). It was stated that melting temperatures of bare Ag NWs were determined as 210, 230 and 260 °C for NW with average diameters of 17, 45 and 120 nm, respectively. It was clear that the melting (degradation) temperature increased with the average diameter of Ag NWs.

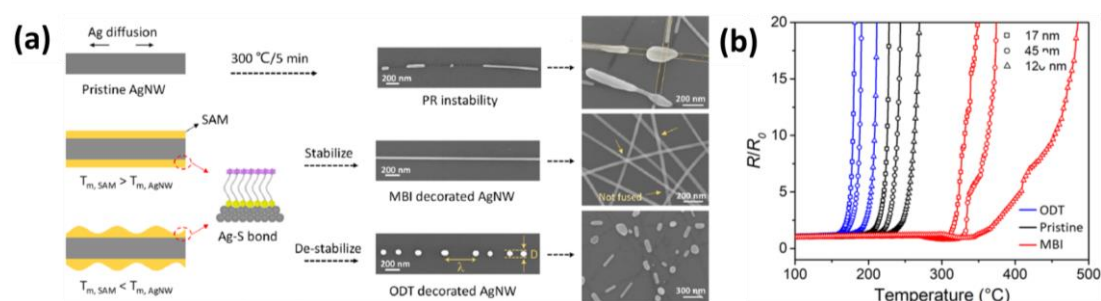


Figure 3. 6 (a) Schematic illustration and SEM images of Ag NWs and coated Ag NWs annealed at 300 for 5 min (b) Resistance change with temperature for Ag NWs with average diameters of 17, 45 and 120 nm [53].

3.1.5. Mechanical Stability

Mechanical stability of Ag NW networks concerns with adhesion of the Ag NW network to the various substrates and bending cycles of networks. As the Ag NW networks withstand even 10000 bending cycles, the main mechanical problem is adhesion to the substrate. When friction or adhesive tape are applied on the Ag NWs networks, it fails due to the low adhesion [54]. To enhance the mechanical stability, there are two main approaches. In the first approaches, the NW networks were created using high nanowire density [55][56].

Transparent polymers and oxides can be coated on the Ag NW networks to improve the adhesion while both the transmittance and resistance remain the similar to those of bare Ag NW network. The most common examples of coating materials are PEDOT:PSS, PDMS, AZO, SnO₂ and ZnO [57][58][59].

3.2. Experimental Procedure

3.2.1. Electrode Preparation

Both bare Ag NW networks and Ag-Pt core-shell NW network (0.47ml of 0.01 M chloroplatinic acid solution) were prepared using spray coating method. Glass and quartz substrates were cleaned via ultrasonication in acetone, ethanol and DI water (for 15 minutes each). Afterwards the substrates were dried using a hot plate set to 120 °C. Suspension of NWs was deposited onto the substrates using spray coating. An air brush was used to spray coat NWs from a distance of 15 cm from the substrate with a pressure of (air brush) 2.5 atm.

3.3. Characterization Methods

3.3.1. Scanning Electron Microscope (SEM)

The prepared electrodes were examined using the field emission scanning electron microscope (FE-SEM) (Nova NanoSEM 430). The operation voltage was 10 kV, 15 kV or 20 kV. The electrodes were attached to grids via double sided carbon tape. Next, gold with a thickness of 2-3 nm was deposited onto the samples via sputtering.

3.3.2. Electrochemical Measurements

A BioLogic 3-channel Electrochemical Workstation (model VMP3) was used to determine the electrochemical properties of the Ag-Pt core-shell NW networks on glass substrates (2.54 x 1.27 cm). One edge of the electrode was painted with carbon colloid used for contacting the samples. Three-electrode configuration was used during the electrochemical measurements where Ag/AgCl was used as the reference electrode, Pt plate was used as the counter electrode and Ag-Pt core-shell NW network electrode was used as the working electrode. The measurements were conducted using a 1 M lithium perchlorate in propylene carbonate (LiClO₄ + PC) as electrolyte.

3.3.3. Relative Humidity

Relative humidity (RH) measurements for the bare and core-shell networks were conducted within glass jar chambers at different humidity levels. In order to set different humidity levels, saturated aqueous suspension of potassium carbonate, sodium chloride and potassium chloride were used to obtain RH values of 43 ± 1 , 75 ± 1 and 84 ± 1 , respectively. RH of the chambers were monitored with a LCD Digital Thermometer Hygrometer Temperature Humidity Meter. The operation limits of the humidity meter were from minus $50\text{ }^{\circ}\text{C}$ to plus $70\text{ }^{\circ}\text{C}$ for temperature and 10 \%RH 99 \%RH with $\pm 5\text{ \%RH}$ accuracy and 1 \%RH resolution for humidity. The chambers were kept at room temperature during the measurements.

3.4. Results

3.4.1. Environmental Stability

Environmental stability of Ag-Pt core-shell NW networks was monitored under high temperatures and at different humidity levels and compared to that of bare Ag NW networks.

3.4.1.1. Temperature Stability

The temperature stability of networks was investigated in such a way that electrodes were placed on a hot plate which was set to $150\text{ }^{\circ}\text{C}$ and $75\text{ }^{\circ}\text{C}$. Room temperature measurements were also taken. $150\text{ }^{\circ}\text{C}$ was maintained for 40 hours, while electrodes were kept in open atmosphere. There was no change in the initial resistance value of the Ag-Pt core-shell NW network. On the other hand, degradation of bare Ag NW network started four hours after beginning of the measurement and complete degradation of the network occurred after 31 hours. Figure 3. 7 (a) shows the change in resistance with respect to time for Ag-Pt core-shell and bare Ag NW networks kept at $150\text{ }^{\circ}\text{C}$.

Stability measurement took 170 hours at $75\text{ }^{\circ}\text{C}$. Figure 3. 7 (b) shows the change in resistance with time for Ag-Pt core-shell and bare Ag NW networks kept at $75\text{ }^{\circ}\text{C}$. As

in the case of 150 °C, change in resistance was not observed for the Ag-Pt core-shell NW network during the measurement. However, the resistance of bare Ag NW network started to increase during the measurement until it totally lost its conductivity.

Lastly, the resistance change was monitored for the networks at room temperature. Figure 3. 7 (c) shows the resistance change with time for Ag-Pt core-shell and bare Ag NWs networks at room temperature. No considerable changes in resistance for Ag-Pt core-shell NW networks was observed at room temperature. On the other hand, the bare Ag NW network started to deteriorate slowly after fabrication of electrode and the resistance became several times that of the initial value after the measurement.

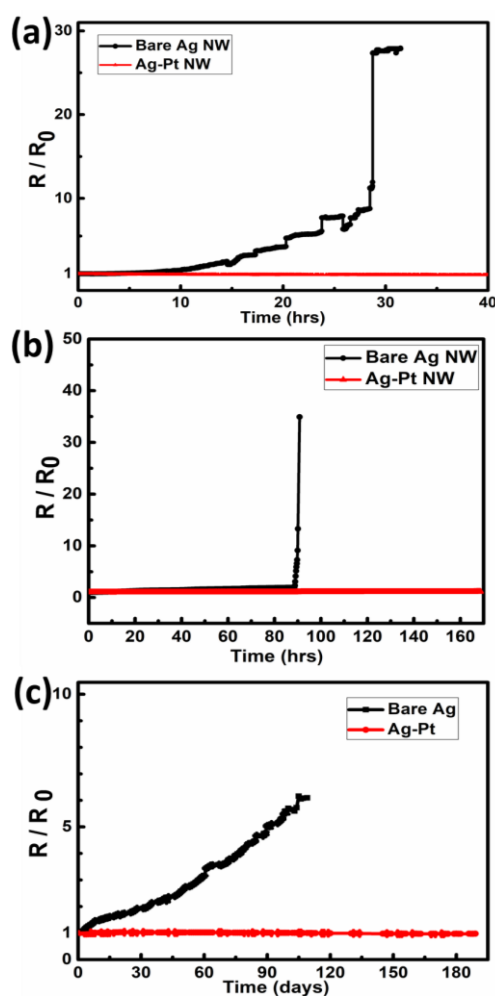


Figure 3. 7 (a) Resistance change with time for 150 °C, (b) 75 °C and (c) room temperature (black lines for bare Ag, red lines for Ag-Pt).

Figure 3. 8 (a) and (b) show the SEM images of the electrodes following temperature measurements at 150 °C for Ag-Pt core-shell and bare Ag NW networks, respectively. Ag-Pt core shell NWs preserved their morphology without fragmentation or melting. However, bare Ag NWs experienced the fragmentation due to the Rayleigh instability, which are shown by the red dashed circles in Figure 3. 8 (b). Figure 3. 8 (c) and (d) show the SEM images of electrodes following temperature measurement at 75 °C for Ag-Pt core-shell NW and bare Ag NW networks, respectively. Conformal coating and smooth surfaces of Ag-Pt core-shell NWs remained after 75 °C measurement. However, the fragmentations of Ag NWs and formation of rough surface were observed, which are shown inside the red dashed circles in Figure 3. 8 (d) took place.

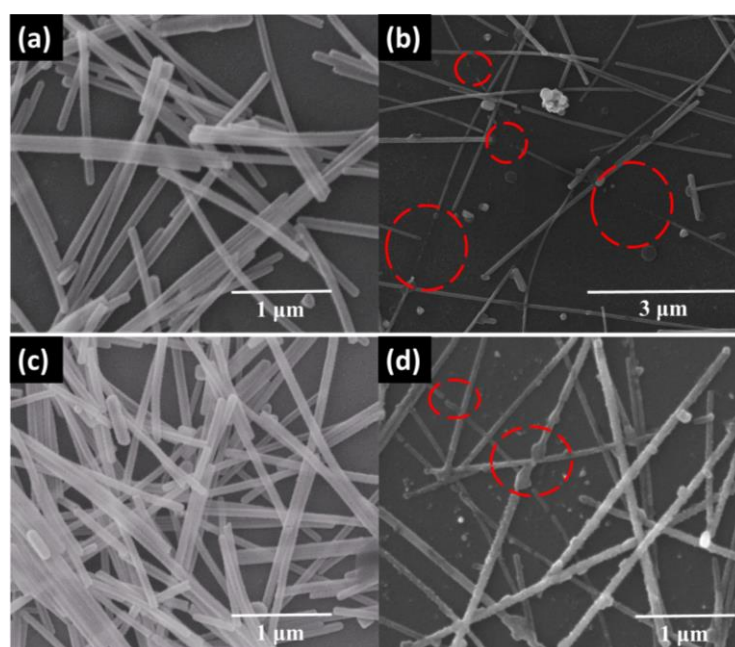


Figure 3. 8 SEM images of electrodes after 150 °C measurement (a) for Ag-Pt core shell NWs and (b) for bare Ag NWs. SEM images of electrodes after 75 °C measurement (a) for Ag-Pt core shell NWs and (b) for bare Ag NWs.

3.4.1.2. Relative Humidity

Figure 3. 9 (a), (b) and (c) provide time dependent resistance changes of Ag NW networks at 85, 75 and 43 %RH levels, respectively, for both pristine Ag NWs networks and Ag-Pt core-shell-nanowire networks. For the cases of 85 %RH and 75 %RH, there was an initial drop in the resistance since the dissolution of PVP with

water occurred due to the extremely humid environment [60]. After decrease in resistance due to the PVP dissolution, the resistance of the electrodes started to increase. On the other hand, increase in the resistance of electrodes at 43 %RH condition started only after they were placed in RH chamber. The results showed that Ag-Pt core-shell-nanowire networks were still durable throughout the whole measurements. On the other hand, the pristine Ag NW networks were failed under 85 and 75 %RH levels. However, Ag NW network kept at 43 %RH level was still conductive although its resistance was increased several times of its initial resistance value.

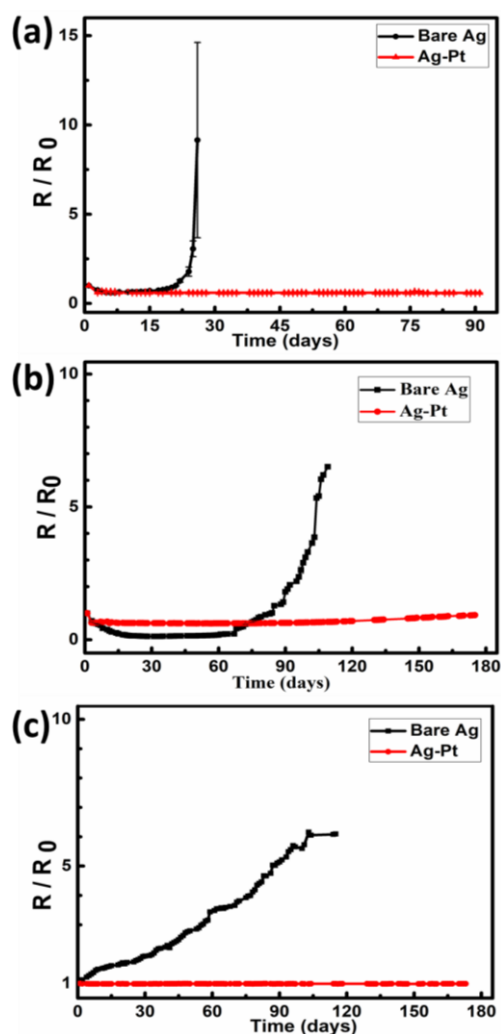


Figure 3. 9 (a) Resistance change with time for 85 %RH , (b) 75 %RH and (c) 43 %RH (black lines for bare Ag, red lines for Ag-Pt).

Figure 3. 10 (a)-(d) show the SEM images for both pristine Ag NW and Ag-Pt core-shell NW electrodes. It is clear that Ag-Pt core-shell NWs maintained their initial morphology in both 85 %RH and 75 %RH conditions. However, Ag NW networks experienced oxidation of Ag. Fragmentation of NWs was also observed, which is marked with red circles in Figure 3. 10 (b) and (d).

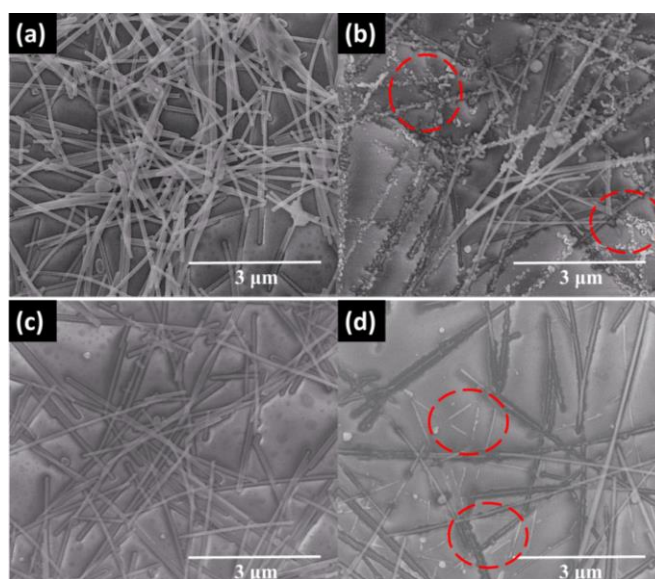


Figure 3. 10 SEM images of electrodes kept in 85% RH (a) for Ag-Pt core shell NWs and (b) for bare Ag NWs, 75 %RH level (c) for Ag-Pt core shell NWs and (d) for bare Ag NWs.

3.4.1.3. Chemical Stability

The chemical stability test was also conducted measuring the resistance change while the nanowire networks were exposed to H_2O_2 10 vol.% of H_2O_2 solution was dropped to the center of the electrodes parallel to the contacts. The resistance of the pristine Ag NW network was increased within the first 10 seconds due to the etching of Ag NWs, shown in Figure 3. 11 (a) and SEM image shows the destroyed Ag NW networks in Figure 3. 11 (c). On the other hand, Ag-Pt core-shell NW networks experienced slight increase in the resistance even after 10000 seconds (about 167 mins) of exposure to H_2O_2 solution. This is also confirmed by the stable resistance measurements. Moreover, SEM image, in Figure 3. 11 (b), also confirmed the protection and stability of NWs since Ag-Pt NWs were seem to be unaffected by the exposure to H_2O_2

solution. Therefore, NW networks were protected from harsh conditions by the Pt coating on Ag NWs.

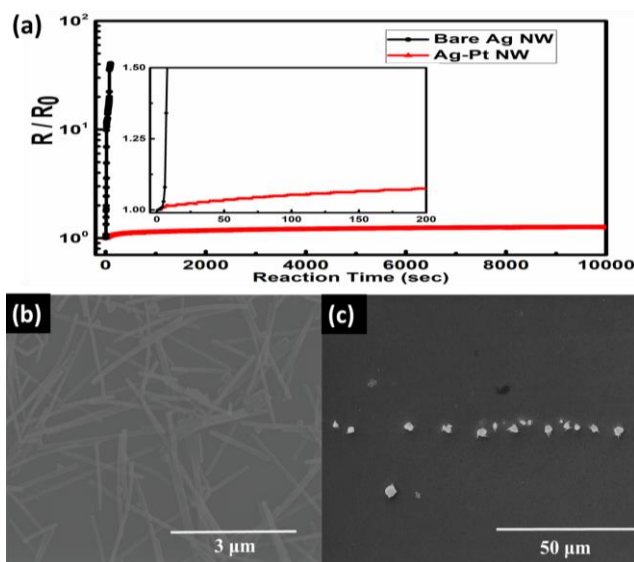


Figure 3. 11 (a) Resistance change with time for H_2O_2 stability measurement (black line for bare Ag, red line for Ag-Pt) (inside is early stage of the measurement), SEM images of electrodes after H_2O_2 treatment (b) for Ag-Pt core shell NWs and (c) for bare Ag NWs (black line for bare Ag, red line for Ag-Pt).

3.4.2. Electrochemical Stability

Having a critical role in electrochemical performance of Ag NWs, evaluating the exact working potential window in which Ag NWs remain stable is of prime significance. Accordingly, electrochemical behavior of the prepared electrodes was investigated in three-electrode configuration using cyclic voltammetry (CV) technique under ambient conditions. The working potential window of the Ag NWs was found with widening the potential window, step by step, until reaching potential window limit. Figure 3. 12 provides clear evidence on decomposition of Ag NWs under applying a potential window 0 and 0.9 V. As seen in Figure 3. 12 by applying a working potential of 0.9 V, an oxidation peak observed at the first cycle (green CV) with a rapid current drop and the reduction peak was vanished in the reverse potential sweep providing convincing evidence of oxidation of Ag. In addition, second cycle (blue curve) is also shown in Figure 3. 12 to prove the decomposition of Ag NWs under applied potential.

The cyclic voltammetry results demonstrated that an irreversible reaction was occurred on the electrode surface as a direct consequence of Ag NW decomposition. For comparison, the electrochemical stability of Ag-Pt core-shell NWs (pink CV) was investigated under the same potential window. As seen in Figure 3. 12, the electrochemical stability of Ag NWs was clearly improved upon Pt deposition onto Ag NWs (0.47 ml of 0.1 M chloroplatinic acid solution).

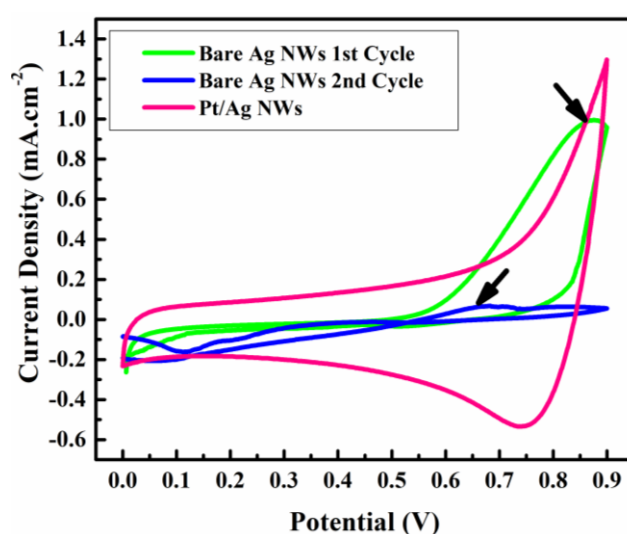


Figure 3. 12 The electrochemical stability of bare Ag NWs (first and second cycles) compared with Ag-Pt core-shell NW networks by applying 0.0-0.9 V.

Supercapacitors offer many advantages compared to conventional energy storage systems (such as high power density and long cycling life). Their low energy density, which arise from their intrinsically narrow potential window plays a critical role in limiting their application. Substantial efforts have been spent to improve the electrochemical and mechanical performance of the Ag NW-based electrodes, seeking a practical strategy still remains to be the greatest challenges yet to be resolved. Herein, Ag NWs were coated with a conformal Pt layer to improve the electrochemical stability Ag NWs. Electrochemical stability of Ag NWs is compared with Pt-coated counterparts in LiClO₄ (1M)-PC electrolyte at a sweep rate of 100 mVs⁻¹. As seen Figure 3. 13, the electrochemical stability of Ag NWs was improved by conformal Pt coating onto Ag NWs.

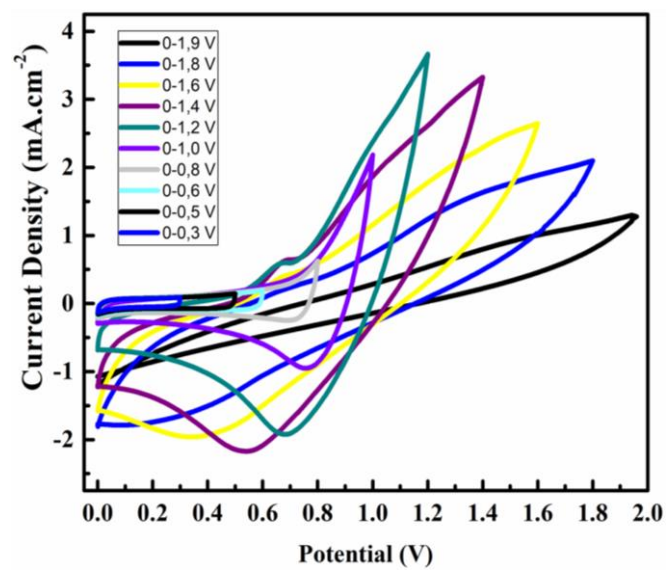


Figure 3. 13 The CVs of Ag-Pt core-shell NWs network under applying different potential windows.

CHAPTER 4

SILVER-PLATINUM CORE-SHELL NANOWIRE NETWORKS BASED THIN FILM HEATERS

4.1. Introduction

Nanowire network electrodes hold great potential to be transparent and conductive components for various applications. In addition to high transparency and low sheet resistance, nanowire network electrodes are also flexible, which paves the way for integration into flexible devices. Due to these superior properties, NW electrodes have been utilized in a wide range of applications. The important examples of these applications include photovoltaics [61], electroluminescent devices [62], electromagnetic devices like shielding and antennas [63] [64], electrochromic devices [65], sensors [66], energy storage systems like supercapacitors and batteries [67] and thin film heaters [68].

Thin film heaters (TFHs) are devices that convert the electrical energy into heat with the mechanism called Joule heating. In other words, the surface of electrode can be heated up through voltage application. TFHs have been utilized in various systems such as microchips, reaction cells, windows defoggers, heating source of sensors, heating substrate of displays and wearable electronics [54]. Most common materials used in TFHs are ITO, FTO, CNT and metal nanowire networks [69]–[74]. Ag NWs have gained significant interest in the last decade due to its high electrical and thermal conductivities [2]. Moreover, Ag NW networks in TFHs respond rapidly to the applied voltage and the temperature distribution on the electrode surface is highly uniform.

4.2. Random Network Formation

Simulation of NW networks to determine the electrical properties was demonstrated by the percolation theory [75][76]. These simulations showed that electrical

conduction of NW networks depend on the NW morphology as well as the length, diameter and network density [8]. The morphology of NWs is primarily important since the optoelectronic properties of the networks play a pivotal role in the applications. NW networks can be formed via various methods such as spray coating, spin coating, dip coating or vacuum transfer and the optoelectronic properties of the network is directly related to the network density. The network density is defined as the number of NWs per unit area and the final optoelectronic performance of the nanowire networks can be controlled by adjusting the network density. Another term is also used in literature to define the mass of metal per unit area (unit of mg/m^2) which is the areal mass density [77], [78]. Generally, optical transparency diminishes as the network density increases. Figure 4. 1 shows experimental results on the change in optical transmittance with respect to areal mass density of Ag NWs with different diameters [78].

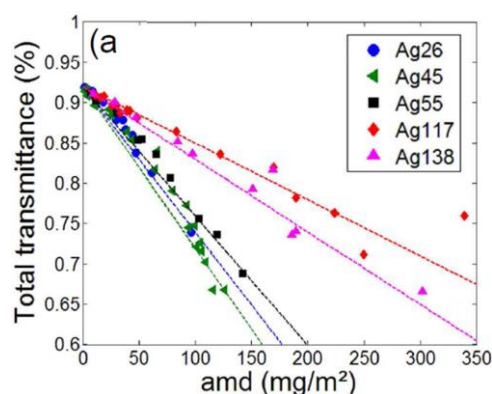


Figure 4. 1 Optical transmittance with respect to areal mass density of Ag NWs with different diameters [78].

4.3. Thin Film Heaters

4.3.1. Working Principles

Heating of TFHs is based on the Joule's law, where the electrical is converted into heat energy under a current flow [79]. The Joule heating of Ag NW networks was defined by Sorel et al. in such a manner that the sample was heated uniformly and energy loss to surroundings was neglected [80]. Then, the energy balance equation was formed in Equation 4.1;

$$I^2R = mC \frac{dT(t)}{dt} + A(h_1 + h_2)(T(t) + T_0) + \sigma A(\varepsilon_1 + \varepsilon_2)(T(t)^4 + T_0^4) \text{ Equation 4.1}$$

,where $T(t)$ and T_0 are the instantaneous and ambient temperatures, A is the area of film (substrate), $m.C$ is the heat capacity (1 for network; 2 for substrate), h_1 and h_2 are the convective heat transfer coefficients for network and substrate, ε_1 and ε_2 are the emissivity of network and substrate, I^2R is the dissipated electrical power.

The electrical power can also be calculated using Ohm's (Equation 4.2) and Joule's (Equation 4.3) Laws;

$$V = I \times R \text{ Equation 4.2}$$

$$P = \frac{V^2}{R} = I^2 \times R = V \times I \text{ Equation 4.3}$$

,where V is the applied potential (volt), R is the resistance (ohm), I is the current (ohm) and P is the electrical power (watt).

In literature, the power density is used to compare the performance of different thin film heaters, which is directly related to the steady-state temperature. The power density is defined as the power per unit area as shown in Equation 4.4 below;

$$\text{Power Density} = \frac{R \times I^2}{A} \text{ Equation 4.4}$$

,where A is the electrode area (cm^2)

The use of Ag NW network electrodes as transparent and flexible heaters was first demonstrated by Celle et al. [68]. Figure 4. 2 shows the heating and cooling curve of Ag NW networks with a sheet resistance of $33 \Omega/\text{sq}$ under different applied voltages of 3, 5 and 7 V. Two prominent features signify the heating behavior. Firstly, there was a linear increase in early stage of the heating and secondly there was a plateau for each applied voltage once the steady-state temperature is reached. Moreover, inset of Figure 4. 2 shows the derivative curve for obtaining the heating and cooling rates. Samples heated up with the rate of $2 \text{ }^\circ\text{C}/\text{sec}$, respectively. The essential point about transparent heaters is that they provide steady state temperature, called as temperature

plateau. This plateau should be attained using minimum potential to reduce the power consumption. Moreover, the response time which is the time to achieve 90 % of the steady state temperature is also required to be as short as possible [79].

Lastly, the morphology of NWs gets destroyed into long chain of nanospheres due to fragmentation at temperatures above 400 °C for NWs with diameters of 30-50 nm. This morphological change is known as the Rayleigh instability, which limits the application of thin metal NWs in heaters at excess temperatures [81].

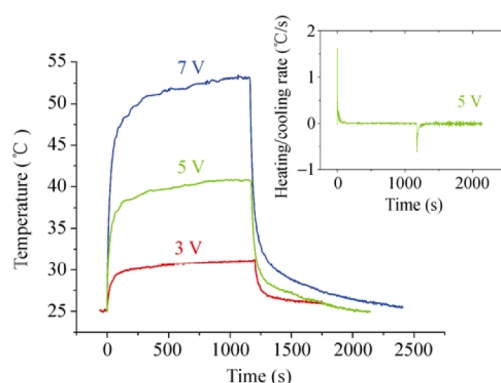


Figure 4. 2 Thermal response of Ag NW networks (inset shows the derivative curve to obtain the heating and cooling rates) [68].

4.3.2. Results from Literature

There have been attempts to encapsulate Ag NW networks to be utilized as transparent heater following the first study [68]. Cheong et al. coated Ag NWs network with aluminum doped zinc oxide (AZO) to reduce the heat loss to surroundings [72]. Figure 4. 3 (a) and (b) shows the heating/cooling curve for bare Ag NW and AZO coated Ag NW networks for applied voltages of 2.25 and 3 V/cm, respectively. In both conditions, AZO coated Ag NW network (shown as white circles) reached higher plateau temperatures than the bare Ag NW network (shown as black squares). The plateau temperature that was obtained at the steady state condition was increased following AZO deposition onto Ag NW networks.

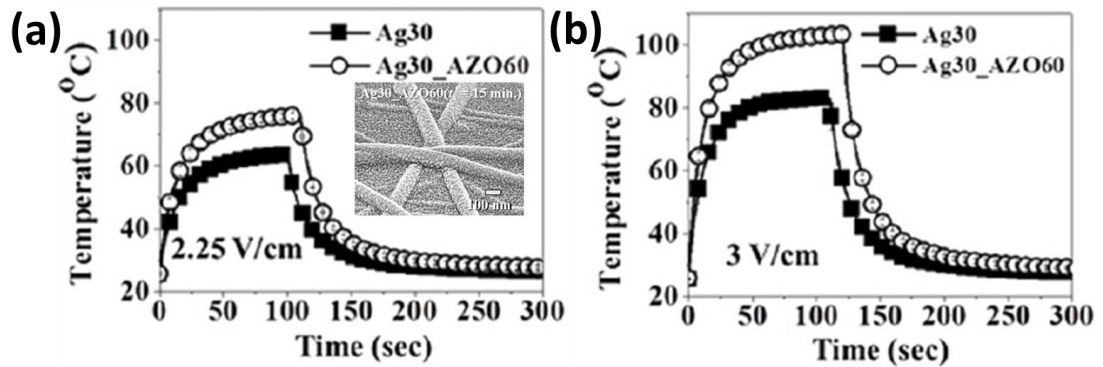


Figure 4. 3 Heating/cooling curve for bare Ag NWs and AZO coated Ag NWs applied potential of (a) 2.25 and (b) for 3 V/cm (inset show SEM image of AZO coated Ag NWs) [72].

Jang et al.[82] investigated the heater performance of the ultra-long silver nanofiber (Ag NF) networks. Figure 4. 4 (a) shows the heating/cooling curves of Ag NFs, Ag NWs and ITO electrodes. Ag NF networks was found to outperform both Ag NW network and ITO based heaters in this work. Figure 4. 4 (b) and (c) show the stepwise increase of voltage form 0.5 to 4.5 V and the corresponding thermal camera images for different applied voltages, respectively.

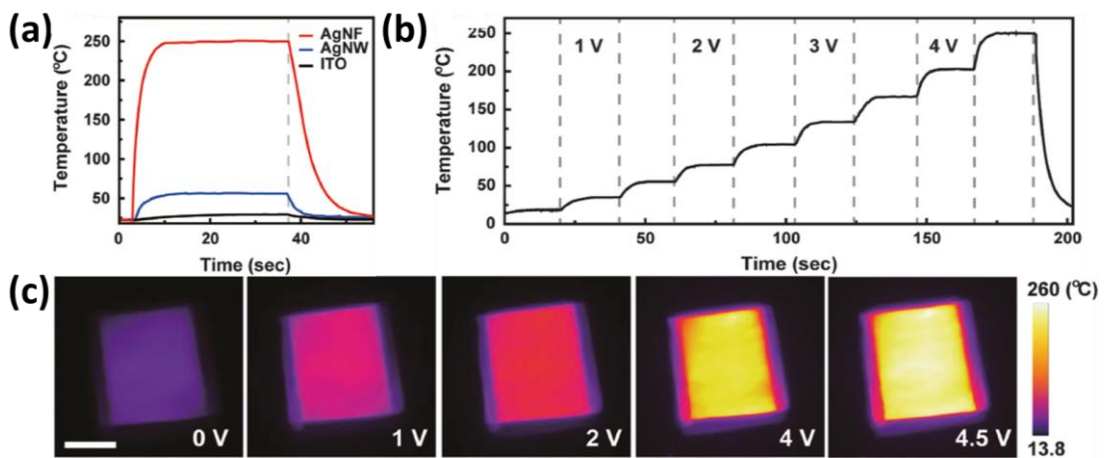


Figure 4. 4 (a) Thermal performance of Ag NWs, Ag NF networks and ITO heaters. (b) Heating/cooling curves during stepwise increase in voltage from 0.5 to 4.5 V. (c) Thermal camera images of Ag NF electrode under different voltages [82].

Lastly, wearable heaters with Ag NWs/PVA film was fabricated by Lan et al.[83]. The thermal performance of ultra flexible and wearable Ag NWs/PVA film heater was investigated. Figure 4. 5 shows the thermal performance of sequential applied voltages

that are 3, 3.5 and 4 V and their photographs while the temperature was being measured with an IR thermometer.

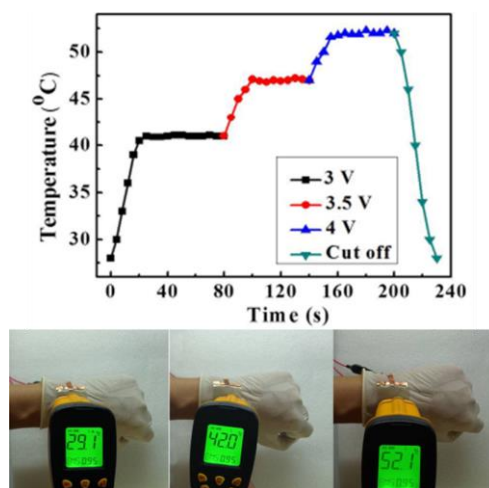


Figure 4. 5 Thermal performance of wearable Ag NWs/PVA film and in-situ temperature measurements [83].

4.4. Experimental Procedure

4.4.1. Electrode Preparation

Both bare Ag NW networks and Ag-Pt core-shell NW networks (0.47ml of 0.01 M chloroplatinic acid solution) were prepared using spray coating method. Glass and quartz substrates were cleaned via ultrasonication in acetone, ethanol and DI water (for 15 minutes each). Afterwards the substrates were dried on a hot plate set to 120 °C. Suspension of NWs was deposited onto these substrates using spray coating. Spray coating parameters were a distance of 15 cm between substrates and tip of air brush, and the pressure of air brush was 2.5 atm for Ag-Pt core-shell and bare Ag NWs.

4.5. Characterization Methods

4.5.1. Scanning Electron Microscope (SEM)

The prepared electrodes were examined using the field emission scanning electron microscope (FE-SEM) (Nova NanoSEM 430). The operation voltage was 10 kV, 15 kV or 20 kV. The samples were attached to SEM stubs using double sided carbon tape.

4.5.2. Thin Film Heater

A silver colloidal paste was applied as two parallel stripes onto the edges of spray coated Ag-Pt core-shell NW electrodes on quartz substrate (2.54 x 2.54 cm). A TT-T-ECHNI DC power supply (model no: MCH-305D-II) was used to apply different potentials between the Ag contacts. Thermal camera imaging was conducted with Optris PI4000 and the temperature values were recorded using a Applent AT4508 multi-channel thermocouple.

4.6. Results

4.6.1. Performance of Thin Film Heaters

The performance of the Ag-Pt core-shell NW network based thin film heaters was monitored using a thermocouple and a thermal camera.

There were changes in the thin film heater (TFH) behavior when applied potential was increased gradually from 10 V to 45 V. With increase in the applied voltage, Ag-Pt core-shell NWs network reached higher temperature values. The temperature distribution was uniform on the electrode surface since NWs were homogeneously deposited onto substrates. Figure 4. 6 (a) and (b) show attained temperature upon stepwise increasing the applied voltage and the corresponding thermal camera images, respectively. The stepwise increase in voltage was applied in such a way that first 10 V was applied and the applied voltage increased 5 V at each step, which took 5 mins. The maximum temperature that was reached without the was 192 °C an applied potential of 45 V (0.09 A) and the temperature dropped suddenly due to the failure of the quartz substrate. The uniform temperature distributions for different applied voltages are clear in the thermal camera images. Then the power and power density were calculated as 4.05 watt and 0.91 watt/cm² according to Equation 4.3 and Equation 4.4 respectively. The Ag-Pt core-shell network was stable at plateau temperature of 192 °C . Calculated power and power density values for all heating steps are shown in . The power density for Ag-Pt core-shell NW network that reached

the maximum temperature is comparable to that in the study by Ergun et al., where 0.99 watt/cm² was consumed to obtain 204 °C [84].

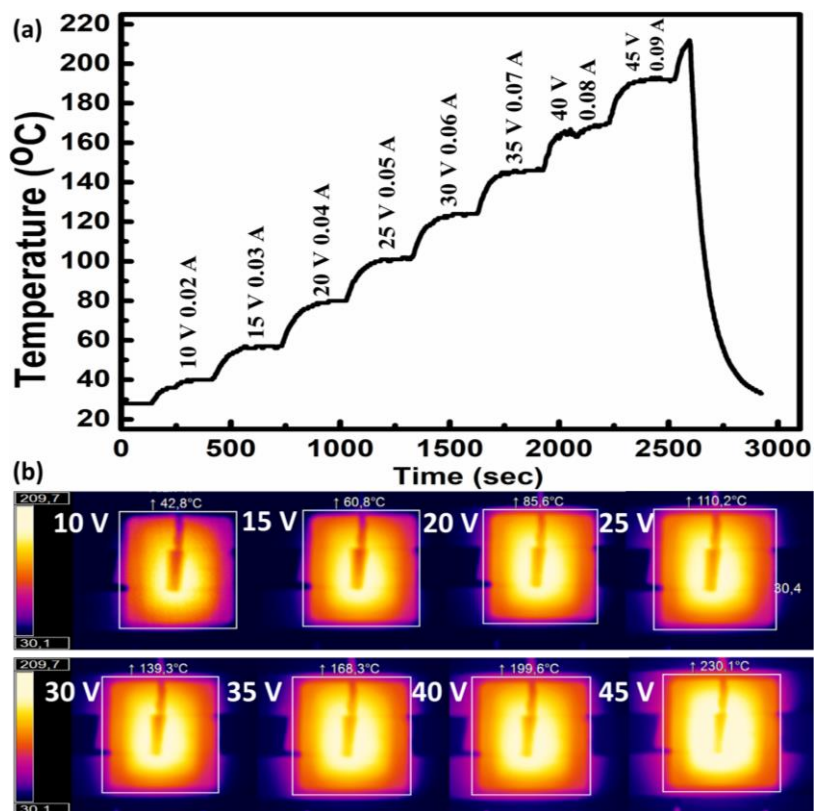


Figure 4. 6 (a) Stepwise heating curve and (b) thermal camera images of stepwise heated Ag-Pt core-shell NW electrodes.

provides the applied voltages, corresponding measured currents and attained temperatures in the stepwise heating and heating/cooling measurements. The response times for each applied voltage are also shown in the table.

Table 4. 1 Measured temperature values for different applied voltages and corresponding current values.

Applied Voltage (V)	Current (A)	Plateau Temperature (Heating/Cooling Curve) (°C)	Power (W)	Power Density (W/cm ²)	Plateau Temperature (Stepwise Heating Curve) (°C)	Response Time (sec)
10	0.02	40	0.20	0.04	54	263
15	0.03	57	0.45	0.10	72	254
20	0.04	80	0.80	0.18	91	302
25	0.05	101	1.25	0.28	112	267
30	0.06	124	1.80	0.40	130	245
35	0.07	146	2.45	0.55	148	264
40	0.08	167	3.20	0.72	169	193
45	0.09	192	4.05	0.91	191	177

Moreover, to show the stability of the TFHs, the continuous heating and cooling cycles with increasing applied voltages were monitored. Figure 4. 7 shows the heating and cooling behavior of Ag-Pt core-shell NW network under different potentials. The response time which is defined as the time to reach steady-state temperature was determined as 177 seconds for applied potential of 45 V (0.09 A). The average response time for 8 different applied potentials is calculated as 245 seconds.

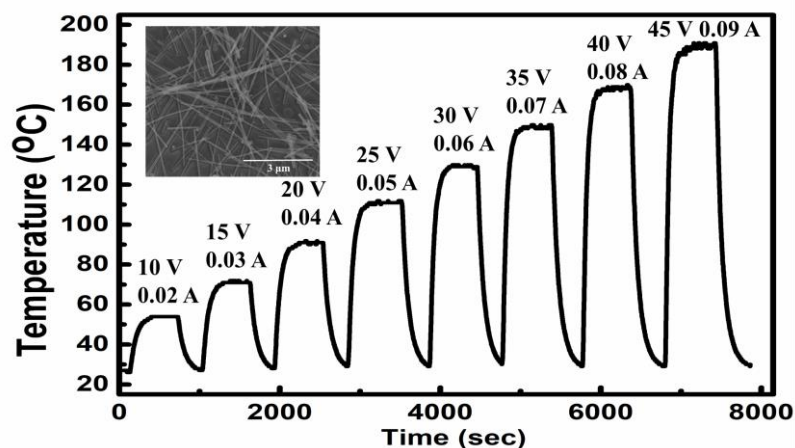


Figure 4. 7 Stepwise heating and cooling of Ag-Pt core-shell NW electrodes (inset shows SEM image of electrode after the measurement).

CHAPTER 5

CONCLUSIONS AND FUTURE RECOMMENDATIONS

5.1. Conclusions

This thesis is focused on the optimization of conformal Pt coating on Ag NW. A solution based method for Pt coating was explored in order to improve electrochemical and electrochemical stability of Ag NWs and Ag NW networks. The characterizations to reveal the conformity and morphology of Ag-Pt core-shell NWs were performed. An optimum chloroplatinic solution concentration (0.01 M 0.47 ml) was determined for the reproducible deposition of a 15-20 nm shell layer around Ag NWs.

The environmental stability of the NW networks was enhanced with Pt coating. The performance of Ag-Pt core-shell NW networks was compared to that of bare Ag NWs in terms of relative humidity stability (43, 75 and 84 % RH), temperature stability (room temperature, 75°C and 150 °C) and stability upon exposure to hydrogen peroxide. For all the cases, Ag-Pt core-shell NW networks were found to outperform bare Ag NW networks.

The electrochemical stability of Ag NW networks was increased such that its narrow potential window was widened after deposition of Pt on Ag NWs. The wider potential window of Ag-Pt core-shell NW networks was determined as 0-1.9 V.

The Ag-Pt core-shell NW electrodes were used as thin film heaters. The maximum temperature that was recorded was 192 °C when 45 V was applied. The corresponding power density was determined as 0.91 watt/cm². The average response time to reach steady-state temperatures was determined as 245 second.

5.2. Future Recommendations

In this thesis, following synthesis, NW networks with enhanced stability were presented. Methods, where the length of the synthesized Ag-Pt core-shell NW are longer than 2-3 μm , should be developed to have higher aspect ratio. The transmittance of Ag-Pt core-shell NW network will certainly be enhanced when Ag-Pt core-shell NWs with high aspect ratio are utilized. Then, Ag-Pt core-shell NW networks can be integrated into the applications as transparent and conductive electrodes.

A further study on this network should involve construction of a device. NW networks can be used as an electrode of a supercapacitor since the potential window was widened. After coating the network with a pseudocapacitive material, a supercapacitor with increased energy and power density can be realized. This pseudocapacitive material can be oxides, sulfides, hydroxides or polymers. Ag-Pt core-shell NW networks can also be integrated as electrodes in a electrochromic devices where a stable NW network is necessary.

Although Ag-Pt core-shell NW network based thin film heaters were studied in this thesis, extensive work should be conducted to determine the best performance of thin film heaters that can be achieved using Ag-Pt core-shell NW networks. The relation between the transmittance and the heater performance of Ag-Pt core-shell NW networks should be revealed.

REFERENCES

- [1] C. Dhand *et al.*, “Methods and strategies for the synthesis of diverse nanoparticles and their applications: A comprehensive overview,” *RSC Adv.*, vol. 5, no. 127, pp. 105003–105037, 2015.
- [2] Y. Shi *et al.*, “Synthesis and Applications of Silver Nanowires for Transparent Conductive Films,” *Micromachines*, vol. 10, no. 5, p. 330, 2019.
- [3] I. M. Sosnin *et al.*, “Synthesis of silver nanochains with a chemical method,” *Mater. Phys. Mech.*, vol. 32, no. 2, pp. 198–206, 2017.
- [4] F. Fievet, J. P. Lagier, B. Blin, B. Beaudoin, and M. Figlarz, “Homogeneous and heterogeneous nucleations in the polyol process for the preparation of micron and submicron size metal particles,” *Solid State Ionics*, vol. 32–33, no. PART 1, pp. 198–205, 1989.
- [5] Y. Sun, B. Gates, B. Mayers, and Y. Xia, “Crystalline Silver Nanowires by Soft Solution Processing,” *Nano Lett.*, vol. 2, no. 2, pp. 165–168, 2002.
- [6] Y. Sun, B. Mayers, T. Herricks, and Y. Xia, “Polyol synthesis of uniform silver nanowires: A plausible growth mechanism and the supporting evidence,” *Nano Lett.*, vol. 3, no. 7, pp. 955–960, 2003.
- [7] A. R. Roosen and W. C. Carter, “Simulations of microstructural evolution: Anisotropic growth and coarsening,” *Phys. A Stat. Mech. its Appl.*, vol. 261, no. 1–2, pp. 232–247, 1998.
- [8] D. Langley, G. Giusti, C. Mayousse, C. Celle, D. Bellet, and J. P. Simonato, “Flexible transparent conductive materials based on silver nanowire networks: A review,” *Nanotechnology*, vol. 24, no. 45, 2013.
- [9] J. Y. Lin, Y. L. Hsueh, J. J. Huang, and J. R. Wu, “Effect of silver nitrate concentration of silver nanowires synthesized using a polyol method and their application as transparent conductive films,” *Thin Solid Films*, vol. 584, pp. 243–247, 2015.
- [10] S. Coskun, B. Aksoy, and H. E. Unalan, “Polyol synthesis of silver nanowires: An extensive parametric study,” *Cryst. Growth Des.*, vol. 11, no. 11, pp. 4963–4969, 2011.

- [11] A. Nekahi, S. P. H. Marashi, and D. H. Fatmesari, "High yield polyol synthesis of round- and sharp-end silver nanowires with high aspect ratio," *Mater. Chem. Phys.*, vol. 184, pp. 130–137, 2016.
- [12] C. Lofton and W. Sigmund, "Mechanisms controlling crystal habits of gold and silver colloids," *Adv. Funct. Mater.*, vol. 15, no. 7, pp. 1197–1208, 2005.
- [13] J. Y. Lin, Y. L. Hsueh, and J. J. Huang, "The concentration effect of capping agent for synthesis of silver nanowire by using the polyol method," *J. Solid State Chem.*, vol. 214, pp. 2–6, 2014.
- [14] H. Yang, T. Chen, H. Wang, S. Bai, and X. Guo, "One-pot rapid synthesis of high aspect ratio silver nanowires for transparent conductive electrodes," *Mater. Res. Bull.*, vol. 102, pp. 79–85, 2018.
- [15] S. Wang, Y. Tian, S. Ding, and Y. Huang, "Rapid synthesis of long silver nanowires by controlling concentration of Cu²⁺ ions," *Mater. Lett.*, vol. 172, pp. 175–178, 2016.
- [16] J. J. Chen *et al.*, "Structural regulation of silver nanowires and their application in flexible electronic thin films," *Mater. Des.*, vol. 154, no. 2017, pp. 266–274, 2018.
- [17] A. Kumar, P. Karadan, and H. C. Barshilia, "Synthesis of silver nanowires towards the development the ultrasensitive AgNWs/SiNPLs hybrid photodetector and flexible transparent conductor," *Mater. Sci. Semicond. Process.*, vol. 75, no. December, pp. 239–246, 2018.
- [18] Z. C. Li, T. M. Shang, Q. F. Zhou, and K. Feng, "Sodium chloride assisted synthesis of silver nanowires," *Micro Nano Lett.*, vol. 6, no. 2, pp. 90–93, 2011.
- [19] T. N. Trung, V. K. Arepalli, R. Gudala, and E. T. Kim, "Polyol synthesis of ultrathin and high-aspect-ratio Ag nanowires for transparent conductive films," *Mater. Lett.*, vol. 194, no. February, pp. 66–69, 2017.
- [20] P. Zhang *et al.*, "Behind the role of bromide ions in the synthesis of ultrathin silver nanowires," *Mater. Lett.*, vol. 213, pp. 23–26, 2018.
- [21] Z. Peng, H. You, and H. Yang, "Composition-dependent formation of platinum silver nanowires," *ACS Nano*, vol. 4, no. 3, pp. 1501–1510, Mar. 2010.
- [22] J. P. Franey, G. W. Kammlott, and T. E. Graedel, "The corrosion of silver by atmospheric sulfurous gases," *Corros. Sci.*, vol. 25, no. 2, pp. 133–143, 1985.

- [23] T. E. Graedel and C. Leygraf, "Corrosion mechanisms for nickel exposed to the atmosphere," *J. Electrochem. Soc.*, vol. 147, no. 3, pp. 1010–1014, 2000.
- [24] V. Gouda, N. A. Ghany, A. Awad, J. Novakovic, and P. Vassiliou, "Silver artifacts protection by anticorrosive coatings," *17th Int. Corros. Congr. 2008 Corros. Control Serv. Soc.*, vol. 2, no. January, pp. 1078–1090, 2008.
- [25] J. L. Elechiguerra, L. Larios-Lopez, C. Liu, D. Garcia-Gutierrez, A. Camacho-Bragado, and M. J. Yacaman, "Corrosion at the nanoscale: The case of silver nanowires and nanoparticles," *Chem. Mater.*, vol. 17, no. 24, pp. 6042–6052, 2005.
- [26] Y. Yang, J. Liu, Z. Fu, and D. Qin, "Galvanic Replacement-Free Deposition of Au on Ag for Core–Shell," *J. Am. Chem. Soc.*, pp. 1–12, 2014.
- [27] H. Lee *et al.*, "Highly Stretchable and Transparent Supercapacitor by Ag-Au Core-Shell Nanowire Network with High Electrochemical Stability," *ACS Appl. Mater. Interfaces*, vol. 8, no. 24, pp. 15449–15458, 2016.
- [28] Y. L. Shen, S. Y. Chen, J. M. Song, and I. G. Chen, "Kinetic study of Pt nanocrystal deposition on Ag nanowires with clean surfaces via galvanic replacement," *Nanoscale Res. Lett.*, vol. 7, no. 1, pp. 1–9, 2012.
- [29] I. E. Stewart, S. Ye, Z. Chen, P. F. Flowers, and B. J. Wiley, "Synthesis of Cu-Ag, Cu-Au, and Cu-Pt Core-Shell Nanowires and Their Use in Transparent Conducting Films," *Chem. Mater.*, vol. 27, no. 22, pp. 7788–7794, 2015.
- [30] R. Yuksel, S. Coskun, and H. E. Unalan, "Coaxial silver nanowire network core molybdenum oxide shell supercapacitor electrodes," *Electrochim. Acta*, vol. 193, pp. 39–44, 2016.
- [31] J. Du, J. Zhang, Z. Liu, B. Han, T. Jiang, and Y. Huang, "Controlled synthesis of Ag/TiO₂ core-shell nano wires with smooth and bristled surfaces via a one-step solution route," *Langmuir*, vol. 22, no. 3, pp. 1307–1312, 2006.
- [32] B. Cheng, Y. Le, and J. Yu, "Preparation and enhanced photocatalytic activity of Ag@TiO₂ core-shell nanocomposite nanowires," *J. Hazard. Mater.*, vol. 177, no. 1–3, pp. 971–977, 2010.
- [33] P. Ramasamy, D. M. Seo, S. H. Kim, and J. Kim, "Effects of TiO₂ shells on optical and thermal properties of silver nanowires," *J. Mater. Chem.*, vol. 22, no. 23, pp. 11651–11657, 2012.

- [34] H. R. Liu *et al.*, “Worm-like Ag/ZnO core-shell heterostructural composites: Fabrication, characterization, and photocatalysis,” *J. Phys. Chem. C*, vol. 116, no. 30, pp. 16182–16190, 2012.
- [35] B. Sciacca, S. A. Mann, F. D. Tichelaar, H. W. Zandbergen, M. A. Van Huis, and E. C. Garnett, “Solution-phase epitaxial growth of quasi-monocrystalline cuprous oxide on metal nanowires,” *Nano Lett.*, vol. 14, no. 10, pp. 5891–5898, 2014.
- [36] S. Vlassov *et al.*, “Shape restoration effect in Ag-SiO₂ core-shell nanowires,” *Nano Lett.*, vol. 14, no. 9, pp. 5201–5205, 2014.
- [37] S. F. Chin, S. C. Pang, and F. E. I. Dom, “Sol-gel synthesis of silver/titanium dioxide (Ag/TiO₂) core-shell nanowires for photocatalytic applications,” *Mater. Lett.*, vol. 65, no. 17–18, pp. 2673–2675, 2011.
- [38] D. Y. Choi, H. W. Kang, H. J. Sung, and S. S. Kim, “Annealing-free, flexible silver nanowire-polymer composite electrodes via a continuous two-step spray-coating method,” *Nanoscale*, vol. 5, no. 3, pp. 977–983, 2013.
- [39] L. R. Shobin and S. Manivannan, “Silver nanowires-single walled carbon nanotubes heterostructure chemiresistors,” *Sensors Actuators, B Chem.*, vol. 256, pp. 7–17, 2018.
- [40] S. K. R. Pillai *et al.*, “Totally embedded hybrid thin films of carbon nanotubes and silver nanowires as flat homogenous flexible transparent conductors,” *Sci. Rep.*, vol. 6, no. November, pp. 1–12, 2016.
- [41] M. xiang Jing, C. Han, M. Li, and X. qian Shen, “High performance of carbon nanotubes/silver nanowires-PET hybrid flexible transparent conductive films via facile pressing-transfer technique,” *Nanoscale Res. Lett.*, vol. 9, no. 1, pp. 1–7, 2014.
- [42] T. Xu *et al.*, “Self-assembly synthesis of silver nanowires/ graphene nanocomposite and its effects on the performance of electrically conductive adhesive,” *Materials (Basel)*, vol. 11, no. 10, 2018.
- [43] F. Alotaibi, T. T. Tung, M. J. Nine, C. J. Coghlan, and D. Losic, “Silver Nanowires with Pristine Graphene Oxidation Barriers for Stable and High Performance Transparent Conductive Films,” *ACS Appl. Nano Mater.*, vol. 1, no. 5, pp. 2249–2260, 2018.
- [44] X. Zhang, X. Yan, J. Chen, and J. Zhao, “Large-size graphene microsheets as a

- protective layer for transparent conductive silver nanowire film heaters,” *Carbon N. Y.*, vol. 69, no. 2, pp. 437–443, 2014.
- [45] Z. Huang *et al.*, “Continuous synthesis of size-tunable silver nanoparticles by a green electrolysis method and multi-electrode design for high yield,” *J. Mater. Chem. A*, vol. 3, no. 5, pp. 1925–1929, 2015.
- [46] Y. Shen, B. Gong, K. Xiao, and L. Wang, “In situ assembly of ultrathin PtRh nanowires to graphene nanosheets as highly efficient electrocatalysts for the oxidation of ethanol,” *ACS Appl. Mater. Interfaces*, vol. 9, no. 4, pp. 3535–3543, 2017.
- [47] M. Giovanni and M. Pumera, “Size Dependant Electrochemical Behavior of Silver Nanoparticles with Sizes of 10, 20, 40, 80 and 107nm,” *Electroanalysis*, vol. 24, no. 3, pp. 615–617, 2012.
- [48] H. Moon *et al.*, “Ag/Au/Polypyrrole Core-shell Nanowire Network for Transparent, Stretchable and Flexible Supercapacitor in Wearable Energy Devices,” *Sci. Rep.*, vol. 7, no. January, pp. 1–10, 2017.
- [49] R. Yuksel, S. Coskun, Y. E. Kalay, and H. E. Unalan, “Flexible, silver nanowire network nickel hydroxide core-shell electrodes for supercapacitors,” *J. Power Sources*, vol. 328, pp. 167–173, 2016.
- [50] J. Jiu *et al.*, “The effect of light and humidity on the stability of silver nanowire transparent electrodes,” *RSC Adv.*, vol. 5, no. 35, pp. 27657–27664, 2015.
- [51] S. Choi *et al.*, “Highly conductive, stretchable and biocompatible Ag–Au core–sheath nanowire composite for wearable and implantable bioelectronics,” *Nat. Nanotechnol.*, vol. 13, no. 11, pp. 1048–1056, 2018.
- [52] “In Reply: BEHAVIOUR THERAPY.” [Online]. Available: <https://www.americanelements.com/meltingpoint.html>. [Accessed: 09-Sep-2019].
- [53] G. S. Liu *et al.*, “Comprehensive Stability Improvement of Silver Nanowire Networks via Self-Assembled Mercapto Inhibitors,” *ACS Appl. Mater. Interfaces*, vol. 10, no. 43, pp. 37699–37708, 2018.
- [54] W. He and C. Ye, “Flexible Transparent Conductive Films on the Basis of Ag Nanowires: Design and Applications: A Review,” *J. Mater. Sci. Technol.*, vol. 31, no. 6, pp. 581–588, 2015.

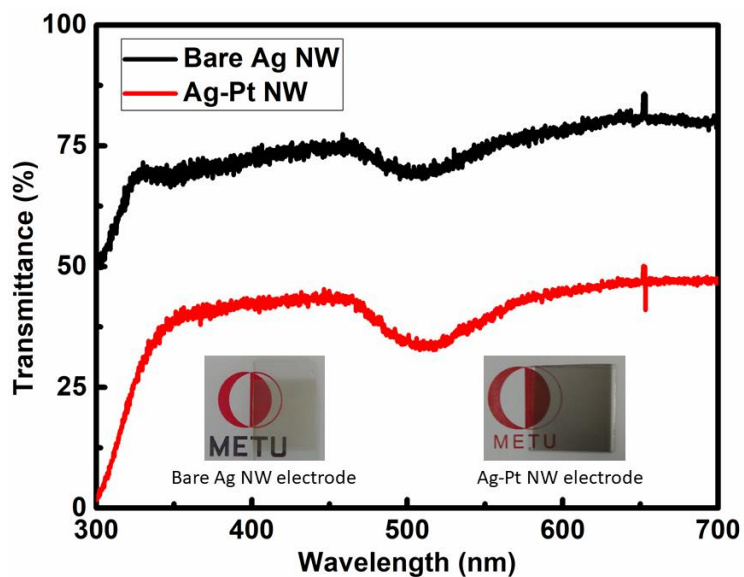
- [55] P. Lee *et al.*, “Highly stretchable and highly conductive metal electrode by very long metal nanowire percolation network,” *Adv. Mater.*, vol. 24, no. 25, pp. 3326–3332, 2012.
- [56] F. Xu and Y. Zhu, “Highly conductive and stretchable silver nanowire conductors,” *Adv. Mater.*, vol. 24, no. 37, pp. 5117–5122, 2012.
- [57] T. Akter and W. S. Kim, “Reversibly stretchable transparent conductive coatings of spray-deposited silver nanowires,” *ACS Appl. Mater. Interfaces*, vol. 4, no. 4, pp. 1855–1859, 2012.
- [58] K. Zilberberg *et al.*, “Highly robust Indium-free transparent conductive electrodes based on composites of silver nanowires and conductive metal oxides,” *Adv. Funct. Mater.*, vol. 24, no. 12, pp. 1671–1678, 2014.
- [59] Y. Jin, D. Deng, Y. Cheng, L. Kong, and F. Xiao, “Annealing-free and strongly adhesive silver nanowire networks with long-term reliability by introduction of a nonconductive and biocompatible polymer binder,” *Nanoscale*, vol. 6, no. 9, pp. 4812–4818, 2014.
- [60] J. Jiu *et al.*, “The effect of light and humidity on the stability of silver nanowire transparent electrodes,” *RSC Adv.*, vol. 5, no. 35, pp. 27657–27664, 2015.
- [61] F. S. F. Morgenstern *et al.*, “Ag-nanowire films coated with ZnO nanoparticles as a transparent electrode for solar cells,” *Appl. Phys. Lett.*, vol. 99, no. 18, pp. 1–4, 2011.
- [62] X. Y. Zeng, Q. K. Zhang, R. M. Yu, and C. Z. Lu, “A new transparent conductor: Silver nanowire film buried at the surface of a transparent polymer,” *Adv. Mater.*, vol. 22, no. 40, pp. 4484–4488, 2010.
- [63] G. A. Gelves, M. H. Al-Saleh, and U. Sundararaj, “Highly electrically conductive and high performance EMI shielding nanowire/polymer nanocomposites by miscible mixing and precipitation,” *J. Mater. Chem.*, vol. 21, no. 3, pp. 829–836, 2011.
- [64] C. Yang *et al.*, “Silver nanowires: From scalable synthesis to recyclable foldable electronics,” *Adv. Mater.*, vol. 23, no. 27, pp. 3052–3056, 2011.
- [65] C. Yan *et al.*, “Stretchable and wearable electrochromic devices,” *ACS Nano*, vol. 8, no. 1, pp. 316–322, 2014.
- [66] S. Yao and Y. Zhu, “Wearable multifunctional sensors using printed stretchable

- conductors made of silver nanowires,” *Nanoscale*, vol. 6, no. 4, pp. 2345–2352, 2014.
- [67] W. Liu, C. Lu, X. Wang, R. Y. Tay, and B. K. Tay, “High-performance microsupercapacitors based on two-dimensional graphene/manganese dioxide/silver nanowire ternary hybrid film,” *ACS Nano*, vol. 9, no. 2, pp. 1528–1542, 2015.
- [68] C. Celle, C. Mayousse, E. Moreau, H. Basti, A. Carella, and J. P. Simonato, “Highly flexible transparent film heaters based on random networks of silver nanowires,” *Nano Res.*, vol. 5, no. 6, pp. 427–433, 2012.
- [69] Z.-S. Zhang, L. Tang, Q.-Y. Ju, L. Ji, M.-H. Zhi, and D.-H. Qiao, “Development of a Heater Structure Based on ITO Films Deposited by RF Magnetron Sputtering for Chip-scale Atomic Clock,” in *Proceedings of the 2nd Annual International Conference on Advanced Material Engineering (AME 2016)*, 2016.
- [70] C. Hudaya, B. J. Jeon, and J. K. Lee, “High Thermal Performance of SnO₂:F Thin Transparent Heaters with Scattered Metal Nanodots,” *ACS Appl. Mater. Interfaces*, vol. 7, no. 1, pp. 57–61, Jan. 2015.
- [71] C. Boo and M. Elimelech, “Carbon nanotubes keep up the heat,” *Nat. Nanotechnol.*, vol. 12, no. 6, pp. 501–503, Jun. 2017.
- [72] H. G. Cheong, J. H. Kim, J. H. Song, U. Jeong, and J. W. Park, “Highly flexible transparent thin film heaters based on silver nanowires and aluminum zinc oxides,” *Thin Solid Films*, vol. 589, pp. 633–641, 2015.
- [73] T. Kim, Y. W. Kim, H. S. Lee, H. Kim, W. S. Yang, and K. S. Suh, “Uniformly interconnected silver-nanowire networks for transparent film heaters,” *Adv. Funct. Mater.*, vol. 23, no. 10, pp. 1250–1255, 2013.
- [74] S. Hong *et al.*, “Highly Stretchable and Transparent Metal Nanowire Heater for Wearable Electronics Applications,” *Adv. Mater.*, vol. 27, no. 32, pp. 4744–4751, 2015.
- [75] I. Balberg, N. Binenbaum, and C. H. Anderson, “Critical behavior of the two-dimensional sticks system,” *Phys. Rev. Lett.*, vol. 51, no. 18, pp. 1605–1608, 1983.
- [76] M. Žeželj, I. Stanković, and A. Belić, “Finite-size scaling in asymmetric systems of percolating sticks,” *Phys. Rev. E - Stat. Nonlinear, Soft Matter Phys.*,

- vol. 85, no. 2, pp. 1–6, 2012.
- [77] S. Lovrics, J. Norton, and W. Taylor, “Society for the Study of Amphibians and Reptiles Cutaneous Myiasis in *Gopherus berlandieri* (Reptilia , Testudines , Testudinidae) Author (s): Raymond W . Neck Reviewed work (s);,” *Society*, vol. 11, no. 1, pp. 96–98, 2012.
- [78] M. Lagrange, D. P. Langley, G. Giusti, C. Jiménez, Y. Bréchet, and D. Bellet, “Optimization of silver nanowire-based transparent electrodes: Effects of density, size and thermal annealing,” *Nanoscale*, vol. 7, no. 41, pp. 17410–17423, 2015.
- [79] T. Sannicolo, M. Lagrange, A. Cabos, C. Celle, J. P. Simonato, and D. Bellet, “Metallic Nanowire-Based Transparent Electrodes for Next Generation Flexible Devices: a Review,” *Small*, vol. 12, no. 44, pp. 6052–6075, 2016.
- [80] S. Sorel, D. Bellet, and J. N. Coleman, “Relationship between material properties and transparent heater performance for both bulk-like and percolative nanostructured networks,” *ACS Nano*, vol. 8, no. 5, pp. 4805–4814, 2014.
- [81] M. E. T. Molaes, A. G. Balogh, T. W. Cornelius, R. Neumann, and C. Trautmann, “Fragmentation of nanowires driven by Rayleigh instability,” *Appl. Phys. Lett.*, vol. 85, no. 22, pp. 5337–5339, 2004.
- [82] J. Jang *et al.*, “Rapid production of large-area, transparent and stretchable electrodes using metal nanofibers as wirelessly operated wearable heaters,” *NPG Asia Mater.*, vol. 9, no. 9, pp. e432–e432, 2017.
- [83] W. Lan *et al.*, “Ultraflexible Transparent Film Heater Made of Ag Nanowire/PVA Composite for Rapid-Response Thermotherapy Pads,” *ACS Appl. Mater. Interfaces*, vol. 9, no. 7, pp. 6644–6651, 2017.
- [84] T. Sannicolo, M. Lagrange, A. Cabos, C. Celle, J. P. Simonato, and D. Bellet, “Metallic Nanowire-Based Transparent Electrodes for Next Generation Flexible Devices: a Review,” *Small*, vol. 12, no. 44, pp. 6052–6075, Nov. 2016.

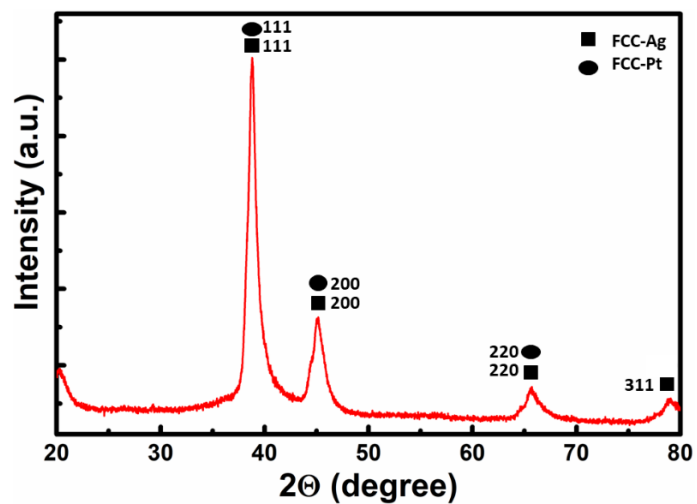
APPENDICES

A. UV-Vis Spectrum



Insets show the photographs of bare Ag (left) and Ag-Pt NW (right) electrodes.

B. XRD Pattern of Ag-Pt Core-Shell NWs



JCPDS Card Numbers are 04-0483 for Ag and 04-0802 for Pt.

C. Heating Rate of Ag-Pt Core-Shell TFHs

